Search for invisible decays of a Higgs boson produced through vector boson fusion in proton-proton collisions at √ s = 13 TeV

Physics Letters B 793 (2019) 520–551

Contents lists available at ScienceDirect

Physics Letters B

www.elsevier.com/locate/physletb

Search for invisible decays of a Higgs boson produced through vector boson fusion in proton-proton collisions at $\sqrt{s} = 13\,\text{TeV}$

The CMS Collaboration *

CERN, Switzerland

ARTICLE INFO

Article history:
Received 16 September 2018
Received in revised form 7 March 2019
Accepted 9 April 2019
Available online 15 April 2019
Editor: M. Doser

Keywords:
CMS
Physics
Higgs
VBF
Invisible decays

ABSTRACT

A search for invisible decays of a Higgs boson is performed using proton-proton collision data collected with the CMS detector at the LHC in 2016 at a center-of-mass energy $\sqrt{s} = 13\,\text{TeV}$, corresponding to an integrated luminosity of $35.9\,\text{fb}^{-1}$. The search targets the production of a Higgs boson via vector boson fusion. The data are found to be in agreement with the background contributions from standard model processes. An observed (expected) upper limit of 0.33 (0.25), at 95% confidence level, is placed on the branching fraction of the Higgs boson decay to invisible particles, assuming standard model production rates and a Higgs boson mass of 125.09 GeV. Results from a combination of this analysis and other direct searches for invisible decays of the Higgs boson, performed using data collected at $\sqrt{s} = 7$, 8, and 13 TeV, are presented. An observed (expected) upper limit of 0.19 (0.15), at 95% confidence level, is set on the branching fraction of invisible decays of the Higgs boson. The combined limit represents the most stringent bound on the invisible branching fraction of the Higgs boson reported to date. This result is also interpreted in the context of Higgs-portal dark matter models, in which upper bounds are placed on the spin-independent dark-matter-nucleon scattering cross section.

1. Introduction

Since the discovery of the Higgs boson at the CERN LHC [1–3], the ATLAS and CMS Collaborations have pursued a wide-ranging program to study its properties and interactions. Precise measurements of the couplings of the Higgs boson to standard model (SM) particles indicate that the properties of the new particle are consistent with the SM predictions [4]. These measurements also provide indirect constraints on additional contributions to the Higgs boson width from beyond the SM (BSM) decays. Based on the results presented in Ref. [4], an indirect upper limit on the Higgs boson branching fraction to BSM particles of 0.34 is set at 95% confidence level (CL).

In the SM, the Higgs boson decays invisibly ($\text{H} \to \text{inv}$) only through the $\text{H} \to \text{ZZ} \to 4\nu$ process, with a branching fraction, $\mathcal{B}(\text{H} \to \text{inv})$, of about 10^{-3}. The rate for invisible decays of the Higgs boson may be significantly enhanced in the context of several BSM scenarios [5–8], including those in which the Higgs boson acts as a portal to dark matter (DM) [9–12]. Direct searches for $\text{H} \to \text{inv}$ decays increase the sensitivity to $\mathcal{B}(\text{H} \to \text{inv})$ beyond the indirect constraints. The ATLAS Collaboration [13] presented a combination of direct searches using $\sqrt{s} = 7$ and 8 TeV data from proton-proton (pp) collisions, yielding an observed (expected) upper limit of 0.25 (0.27) on $\mathcal{B}(\text{H} \to \text{inv})$ at 95% CL [14]. The CMS Collaboration [15] performed a similar combination based on $\sqrt{s} = 7$, 8, and 13 TeV pp collision data collected up to the end of 2015, setting an observed (expected) upper limit of 0.24 (0.23) on $\mathcal{B}(\text{H} \to \text{inv})$ at 95% CL [16].

This Letter presents a search for invisible decays of a Higgs boson, using pp collision data at $\sqrt{s} = 13\,\text{TeV}$ collected with the CMS detector in 2016, corresponding to an integrated luminosity of $35.9\,\text{fb}^{-1}$. The search targets events in which a Higgs boson is produced in association with jets from vector boson fusion (VBF), as illustrated by the Feynman diagram in Fig. 1 (left). In these events, a Higgs boson is produced along with two jets that exhibit a large separation in pseudorapidity ($|\Delta\eta_{\text{jj}}|$) and a large dijet invariant mass (m_{jj}). This characteristic signature allows for the suppression of SM backgrounds, making the VBF channel the most sensitive mode for invisible decays of a Higgs boson at hadron colliders [16, 17]. The invisible particles produced by the Higgs boson decay can recoil with high transverse momentum (p_{T}) against the visible VBF-jet system, resulting in an event with large p_{T} imbalance, which can be used to select signal enriched regions. In this phase

* *E-mail address:* cms-publication-committee-chair@cern.ch.

https://doi.org/10.1016/j.physletb.2019.04.025

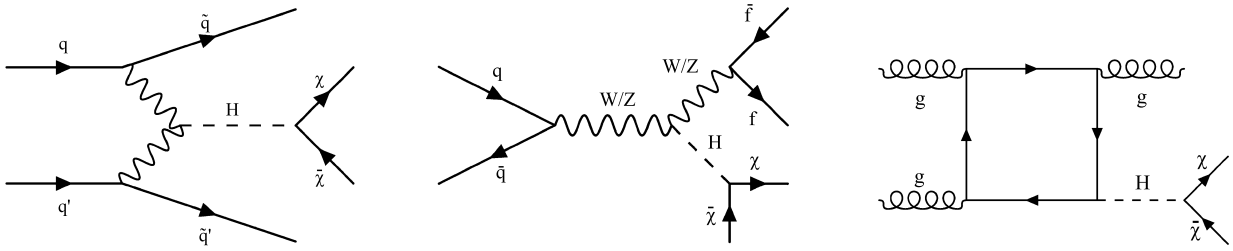

Fig. 1. Leading order Feynman diagrams for the main production processes targeted in the combination: VBF (left), VH (middle), and ggH (right).

space, the main expected backgrounds originate from $Z(\nu\overline{\nu})$+jets and $W(\ell\nu)$+jets processes. They are estimated from data using dedicated control regions (CRs), which consist of high purity samples of Z or W bosons decaying leptonically ($\ell = \mu, e$). While earlier searches probing this final state at the LHC were based on counting experiments, the analysis presented in this Letter more optimally exploits the distinctive kinematic features of the VBF topology by fitting the shape of the m_{jj} distribution. This approach is referred to as the "shape analysis". The shape analysis has been designed to provide a substantially improved sensitivity to invisible decays of the SM Higgs boson, resulting in the most sensitive VBF $H \to$ inv search reported to date. In addition, a simple but less sensitive counting approach, referred to as the "cut-and-count analysis", allows for an easier interpretation of the results of this search in the context of other phenomenological models predicting the same final-state signature. Upper limits on the product of the cross section and branching fraction for an additional Higgs boson with SM-like couplings, which does not mix with the 125 GeV Higgs boson, are also reported.

To further improve the sensitivity, results from a combination of searches for invisible decays of the Higgs boson, using data collected at $\sqrt{s} = 7$, 8, and 13 TeV, are also presented. The searches considered in this combination target the VBF, the associated production (denoted by VH, where V denotes a W or Z boson), and the gluon fusion modes, whose representative Feynman diagrams are shown in Fig. 1. The VH-tag includes both a search for ZH production, in which the Z boson decays to a pair of leptons (e, μ) or b quarks, and one where a Lorentz-boosted W or Z boson decays to light-flavor quarks, whose corresponding hadronization products are reconstructed as a single large-radius jet. Additional sensitivity is achieved by including a search for $gg \to gH$ production (hereafter referred to as ggH), where a high-p_T Higgs boson candidate is produced in association with jets from initial-state radiation. When these searches are combined to set an upper limit on $\mathcal{B}(H \to \text{inv})$, SM production cross sections are assumed. The result of this combination is also interpreted in the context of Higgs-portal models of DM interactions [9–12], in which the 125 GeV Higgs boson plays the role of a mediator between the SM and DM particles, thereby allowing for the possibility of producing DM candidates.

This Letter is organized as follows: after a brief description of the CMS detector in Section 2, the event reconstruction in Section 3, and the simulated signal and background processes in Section 4, Section 5 is dedicated to the event selection requirements followed by a detailed description of the analysis strategy in Section 6. Section 7 reports the results of the VBF search in terms of upper limits on $\mathcal{B}(H \to \text{inv})$. Section 8 reports the upper limit on $\mathcal{B}(H \to \text{inv})$ from a combination of the aforementioned searches for invisible decays of the Higgs boson based on 13 TeV data collected in 2016 while, in Section 9, results from a more complete combination, involving also similar analyses performed on the 7 and 8 TeV data sets, are presented. The Letter is summarized in Section 10.

2. The CMS detector

The CMS detector is a multi-purpose apparatus designed to study a wide range of physics processes in both pp and heavy ion collisions. The central feature of the experiment is a superconducting solenoid of 6 m internal diameter, providing a magnetic field of 3.8 T parallel to the beam direction. Within the solenoid volume a silicon pixel and strip tracker, a lead tungstate crystal electromagnetic calorimeter (ECAL), and a brass and scintillator hadron calorimeter (HCAL) are installed, each composed of a barrel and two endcap sections. The tracker system measures the momentum of charged particles up to $|\eta| = 2.5$, while the ECAL and HCAL provide coverage up to $|\eta| = 3.0$. In addition, the steel and quartz-fiber Cherenkov hadron forward calorimeter extends the coverage to $|\eta| = 5.0$. Muons are detected in gas-ionization chambers embedded in the steel flux-return yoke outside the solenoid, which cover up to $|\eta| = 2.4$.

Events of interest are selected using a two-tiered trigger system [18]. The first level (L1) is composed of custom hardware processors, which use information from the calorimeters and muon detectors to select events at a rate of about 100 kHz. The second level, known as high-level trigger (HLT), is a software-based system which runs a version of the CMS full event reconstruction optimized for fast processing, reducing the event rate to about 1 kHz.

A more detailed description of the CMS detector, together with a definition of the coordinate system used and the relevant kinematic variables, can be found in Ref. [15].

3. Event reconstruction

The particle-flow (PF) algorithm [19] aims to reconstruct and identify each particle in an event with an optimized combination of information from the various elements of the CMS detector. The energy of photons is obtained from the ECAL measurement. The energy of electrons is determined from a combination of the momentum of the associated track at the primary interaction vertex, the energy of the corresponding ECAL cluster, and the energy sum of all bremsstrahlung photons spatially compatible with originating from the electron track. The momentum of muons is obtained from the curvature of the corresponding tracks. The energy of charged hadrons is determined from a combination of their momentum measured in the tracker and the matched ECAL and HCAL energy deposits, corrected for the response function of the calorimeters to hadronic showers. Finally, the energy of neutral hadrons is obtained from the corresponding corrected ECAL and HCAL energy.

The missing transverse momentum vector ($\vec{p}_T^{\,\text{miss}}$) is computed as the negative vector p_T sum of all the PF candidates in an event, and its magnitude is denoted as p_T^{miss}. Hadronic jets are reconstructed by clustering PF candidates using the anti-k_T algorithm [20,21], with a distance parameter of 0.4. The reconstructed vertex with the largest value of summed physics object p_T^2 is taken to be the primary pp interaction vertex, where physics objects correspond to the jets and the p_T^{miss} measured in the event.

The charged PF candidates originating from any other vertex are ignored during the jet finding procedure. Jet momentum is determined as the vector sum of all particle momenta inside the jet, and is found from simulation to vary, on average, between 5 and 10% of the true momentum over the whole p_T spectrum and detector acceptance. An offset correction is applied to jet energies to take into account the contribution from additional pp interactions within the same or adjacent bunch crossings (pileup) [22]. Jet energy corrections are derived from simulation and are confirmed with *in situ* measurements of the energy balance in dijet, multijet, γ+jets, and leptonically decaying Z+jets events [23]. These energy corrections are also propagated to the p_T^{miss} calculation [24].

Muon candidates, within the geometrical acceptance of the silicon tracker and muon subdetectors ($|\eta| < 2.4$), are reconstructed by combining the information from the tracker and the muon chambers [25]. These candidates are required to satisfy a set of quality criteria based on the number of hits measured in the tracker and the muon system, the properties of the fitted muon track, as well as the impact parameters of the track with respect to the primary vertex of the event.

Electron candidates within $|\eta| < 2.5$ are reconstructed using an algorithm that associates fitted tracks in the silicon tracker with electromagnetic energy clusters in the ECAL [26]. To reduce the misidentification rate, these candidates are required to satisfy identification criteria based on the shower shape of the energy deposit, the matching of the electron track to the ECAL energy cluster, the relative amount of energy deposited in the HCAL detector, and the consistency of the electron track with the primary vertex. Because of non-optimal reconstruction performance, electron candidates in the transition region between the ECAL barrel and endcap, $1.44 < |\eta| < 1.57$, are not considered in the analysis. Electrons identified as coming from photon conversions in the detector are discarded [27].

Identified electrons or muons are required to be isolated from hadronic activity in the event. The isolation is defined by summing the p_T of all the PF candidates within a cone of radius $R = \sqrt{(\Delta\eta)^2 + (\Delta\phi)^2} = 0.4\,(0.3)$ around the muon (electron) track, and is corrected for the contribution of neutral hadrons from pileup interactions [25,26].

Hadronically decaying τ leptons (τ_h) are identified from reconstructed jets via the hadron-plus-strip algorithm [28], that requires a subset of particles inside the jet to be consistent with the decay products of a τ lepton. In addition, the τ_h candidate must be isolated from other activity in the detector. The isolation is computed by summing the p_T of all the charged PF candidates and PF photons within a cone of radius $R = 0.3$ around the jet axis. Hadronic τ leptons are selected with an average efficiency between 60 and 65%.

4. Simulated samples

The signal and background processes are simulated using several Monte Carlo (MC) generators. Higgs boson signal events, produced through ggH and VBF, are generated with POWHEG v2.0 [29–33] at next-to-leading order (NLO) approximation in perturbative quantum chromodynamics (QCD). Signal events are normalized to the inclusive Higgs boson production cross sections taken from the recommendations of Ref. [34]. The ggH production cross section is computed at next-to-next-to-NLO (N^3LO) precision in QCD, and at NLO in electroweak (EW) theory [35]. The cross section for Higgs boson production through VBF is calculated at next-to-NLO (NNLO) in QCD, including also NLO EW corrections. The ggH process is simulated using calculations in which the top quark loop is fully resolved. The p_T distribution of the Higgs boson produced via ggH is reweighted to match the NNLO plus next-to-next-to-leading-logarithmic (NNLL) prediction from HRES v2.1 [36, 37]. When upper limits are set on $\mathcal{B}(H \to inv)$ for the SM Higgs boson, both ggH and VBF signal events are generated assuming a Higgs boson mass of 125.09 GeV, which is consistent with the combined ATLAS and CMS measurement [38] based on 7+8 TeV data, as well as the recent CMS measurement at 13 TeV in the $H \to ZZ \to 4\ell$ channel [39].

The $Z/\gamma^*(\ell^+\ell^-)$+jets, $Z(\nu\overline{\nu})$+jets, and $W(\ell\nu)$+jets backgrounds are simulated at leading order (LO) using MADGRAPH5_aMC@NLO v2.2.2 [40], where up to four partons in the final state are included in the matrix element calculation. The background processes involving the production of a vector boson (V) in association with two jets exclusively through EW interactions, i.e. of order α^4, are simulated at LO via MADGRAPH5_aMC@NLO. In addition, the QCD multijet background is also simulated at LO using MADGRAPH5_aMC@NLO. The $t\bar{t}$ and single top quark background samples are produced at NLO QCD using POWHEG v2.0 and v1.0, respectively [41–43]. Finally, the WZ and ZZ diboson productions are simulated at LO with PYTHIA v8.205 [44], while the Vγ and WW processes are simulated at NLO QCD using MADGRAPH5_aMC@NLO and POWHEG [45], respectively.

In all cases, generated events are interfaced with PYTHIA v8.205 or higher for the simulation of fragmentation, parton showering, and the underlying event description, using the parameters from the CUETP8M1 tune [46]. In the case of LO (NLO) MADGRAPH5_aMC@NLO samples, partons from the matrix elements are matched to the parton shower description via the MLM [47] (FxFx [48]) scheme. The NNPDF v3.0 [49] parton distribution functions (PDFs) are used for all the matrix element calculations. Interactions of the final-state particles with the CMS detector are simulated with GEANT4 [50]. Simulated events include the effects of pileup, and are weighted to reproduce the observed pileup distribution.

5. Event selection

Events in the signal region (SR) are selected initially by the L1 trigger exploiting the p_T^{miss} information, whose threshold varies between 60 and 90 GeV depending on the instantaneous luminosity. The p_T^{miss} at the L1 trigger is computed from the vector p_T sum of all the energy depositions in the calorimeters with $|\eta| < 3$. Partial mistiming of signals in the forward region of the ECAL endcaps ($2.5 < |\eta| < 3.0$) led to a reduction in the L1 trigger efficiency. A correction for this effect was determined using an unbiased data sample. This correction was found to be about 1% for m_{jj} of 200 GeV and it increases to about 20% for m_{jj} larger than 3.5 TeV.

At the HLT level, events of interest are collected using triggers with thresholds of 110 or 120 GeV, depending on the data taking period, applied equally to both the missing transverse momentum computed at the trigger level ($p_{T,\,trig}^{miss}$) and the $H_{T,\,trig}^{miss}$ variable. The $H_{T,\,trig}^{miss}$ is defined as the magnitude of the vector p_T sum of the reconstructed jets at the trigger level in the event with $p_T > 20$ GeV and $|\eta| < 5$. The energy fraction attributed to neutral hadrons in jets with $|\eta| < 3.0$ is required to be less than 90%, in order to remove spurious jets originating from detector noise. Both $p_{T,\,trig}^{miss}$ and $H_{T,\,trig}^{miss}$ are calculated without including muon candidates, allowing the same triggers to be used also for selecting events in the muon CRs, which are used in the background estimation procedure described in Section 6.

Offline, events considered in the VBF search are required to have at least two jets with p_T larger than 80 (40) GeV for the leading (subleading) jet. Since the L1 trigger decision does not

Table 1
Summary of the kinematic selections used to define the SR for both the shape and the cut-and-count analyses.

Observable	Shape analysis	Cut-and-count analysis	Target background
Leading (subleading) jet	$p_T > 80\,(40)$ GeV, $\|\eta\| < 4.7$		All
p_T^{miss}	>250 GeV		QCD multijet, $t\bar{t}$, γ+jets, V+jets
$\Delta\phi(\vec{p}_T^{miss}, \vec{p}_T^{jet})$	>0.5 rad		QCD multijet, γ+jets
Muons (electrons)	$N_{\mu,e} = 0$ with $p_T > 10$ GeV, $\|\eta\| < 2.4\,(2.5)$		W($\ell\nu$)+jets
τ_h candidates	$N_{\tau_h} = 0$ with $p_T > 18$ GeV, $\|\eta\| < 2.3$		W($\ell\nu$)+jets
Photons	$N_\gamma = 0$ with $p_T > 15$ GeV, $\|\eta\| < 2.5$		γ+jets, Vγ
b quark jet	$N_{jet} = 0$ with $p_T > 20$ GeV, CSVv2 > 0.848		$t\bar{t}$, single top quark
$\eta_{j1}\,\eta_{j2}$	<0		Z($\nu\bar{\nu}$)+jets, W($\ell\nu$)+jets
$\|\Delta\phi_{jj}\|$	<1.5 rad		Z($\nu\bar{\nu}$)+jets, W($\ell\nu$)+jets
$\|\Delta\eta_{jj}\|$	>1	>4	Z($\nu\bar{\nu}$)+jets, W($\ell\nu$)+jets
m_{jj}	>200 GeV	>1.3 TeV	Z($\nu\bar{\nu}$)+jets, W($\ell\nu$)+jets

use information from the hadronic activity in the forward region, at least one of the two leading jets in the event is required to have $|\eta| < 3$. To ensure a high and stable trigger efficiency, events are further required to have $p_T^{miss} > 250$ GeV. The trigger efficiency is measured as a function of H_T^{miss}, computed from jets with $p_T > 30$ GeV and $|\eta| < 3$. After correcting for the L1 mistiming inefficiency, these triggers are found to be fully efficient for events passing the analysis selection with $H_T^{miss} > 250$ GeV. In addition, if the leading jet is within the geometrical acceptance of the tracker ($|\eta| < 2.4$), its energy fraction attributed to charged hadrons is required to be greater than 10%, while the energy fraction attributed to neutral hadrons is required to be smaller than 80%. These requirements, along with quality filters applied to tracks, muon candidates, and other physics objects, reduce the contamination arising from large misreconstructed p_T^{miss} from noncollision backgrounds [51]. To further suppress the contamination from QCD multijet events, in which a large p_T^{miss} may arise from a severe mismeasurement of the jet momentum, the jets in the event, with $p_T > 30$ GeV and $|\eta| < 4.7$, are required to not be aligned with the $\vec{p}_T^{miss}$. The minimum value of the azimuthal angle between the $\vec{p}_T^{miss}$ vector and each jet ($\min\Delta\phi(\vec{p}_T^{miss}, \vec{p}_T^{jet})$) is required to be larger than 0.5 rad, where only the first four leading jets are included in the $\min\Delta\phi(\vec{p}_T^{miss}, \vec{p}_T^{jet})$ definition. This selection reduces the QCD multijet contamination to less than 1% of the total background.

The two leading jets in VBF signal events typically show a large separation in η, large m_{jj} and a small azimuthal separation ($|\Delta\phi_{jj}|$). The discriminatory power of $|\Delta\phi_{jj}|$ results from a combination of the spin-parity properties of the Higgs boson and the high-p_T regime explored by this search [17], in which the two VBF jets tend to recoil against the invisible system. The Z($\nu\bar{\nu}$)+jets and W($\ell\nu$)+jets processes constitute the largest backgrounds in this search. The shape analysis primarily employs the large separation power of m_{jj} to discriminate between VBF signal and V+jets backgrounds. Therefore, in this scenario, a set of loose requirements is applied on both m_{jj} and $|\Delta\eta_{jj}|$, i.e. $|\Delta\eta_{jj}| > 1.0$ and $m_{jj} > 200$ GeV. To further reduce the V+jets contamination, $|\Delta\phi_{jj}|$ is required to be smaller than 1.5 rad and the two jets must lie in opposite hemispheres, $\eta_{j1}\,\eta_{j2} < 0$. In the cut-and-count approach, Z($\nu\bar{\nu}$)+jets and W($\ell\nu$)+jets processes are suppressed by a more stringent event selection requiring $|\Delta\eta_{jj}| > 4.0$ and $m_{jj} > 1.3$ TeV, while the requirement applied on $|\Delta\phi_{jj}|$ remains unchanged.

The W($\ell\nu$)+jets background is further suppressed by rejecting events that contain at least one isolated electron or muon with $p_T > 10$ GeV, or a τ_h candidate with $p_T > 18$ GeV and $|\eta| < 2.3$, where the isolation is required to be less than 25 (16)% of the muon (electron) p_T. With this strategy, prompt muons (electrons) are selected with an average efficiency of about 98 (95)%. In order to further reduce the contribution from γ+jets and Vγ processes, events containing an isolated photon with $p_T > 15$ GeV and $|\eta| < 2.5$, passing identification criteria based on its ECAL shower shape [27], are vetoed.

Top quark backgrounds ($t\bar{t}$ and single top quark processes) are suppressed by rejecting events in which at least one jet, with $p_T > 20$ GeV and $|\eta| < 2.4$, is identified as a b quark jet using the combined secondary vertex (CSVv2) algorithm [52]. A working point that yields a 60% efficiency for tagging a b quark jet and a 1 (10)% probability of misidentifying a light-flavor (c quark) jet as a b quark jet is used.

A summary of the selection criteria for the SR for both the shape and the cut-and-count analyses is shown in Table 1.

6. Analysis strategy

The search exploits the large m_{jj} and $|\Delta\eta_{jj}|$ that characterize events from VBF Higgs boson production. In the shape analysis case, the signal is extracted by fitting the sum of the signal and background shapes to the binned m_{jj} distribution observed in data. The signal is expected to accumulate as an excess of events over the background at large values of m_{jj}. This strategy necessitates a precise estimation of the shape of the background m_{jj} distribution.

About 95% of the total expected background in this search is due to the V+jets processes, namely Z($\nu\bar{\nu}$)+jets and W($\ell\nu$)+jets. A fraction of the V+jets background, referred to as V+jets (EW), can be attributed to the EW production of a Z or a W boson in association with two jets. A representative Feynman diagram contributing to V+jets (EW) production is shown in Fig. 2 (left). The remaining V+jets contribution arises from the production of a vector boson in association with QCD radiation, as shown in Fig. 2 (right). This is referred to as the V+jets (QCD) background. For both EW and QCD productions, the expected Z($\nu\bar{\nu}$)+jets rate in the SR is about two times larger than the W($\ell\nu$)+jets contribution.

A comparison of the shapes of the key discriminating observables used in this analysis, obtained after applying the requirements listed in Table 1 except for those on m_{jj}, $|\Delta\eta_{jj}|$ and $|\Delta\phi_{jj}|$, is shown in Fig. 3 for simulated signal and V+jets background events. From these distributions, it can be seen that the V+jets (EW) background is kinematically similar to the VBF Higgs boson signal. Therefore, its contribution to the total V+jets background rate increases when the two leading jets have large m_{jj} and $|\Delta\eta_{jj}|$. The V+jets (EW) process constitutes about 2% of the total V+jets background for m_{jj} around 200 GeV. Its contribution increases to about 20% for $m_{jj} \approx 1.5$ TeV, and is more than 50% for $m_{jj} > 3$ TeV.

6.1. Overview of the V+jets background estimation

The Z+jets and W+jets backgrounds are estimated using four mutually exclusive CRs. These include a dimuon and a dielectron

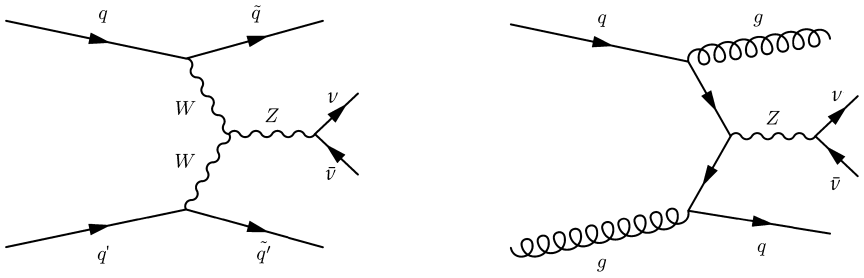

Fig. 2. Representative leading order Feynman diagrams for the production of a Z boson in association with two partons arising from EW (left) and QCD (right) interactions. The left diagram contributes to the Z($\nu\overline{\nu}$)+jets (EW) production cross section, while the diagram on the right to the Z($\nu\overline{\nu}$)+jets (QCD) one. Diagrams for EW and QCD production of a W boson in association with two jets are similar to those reported above for the Z($\nu\overline{\nu}$)+jets process.

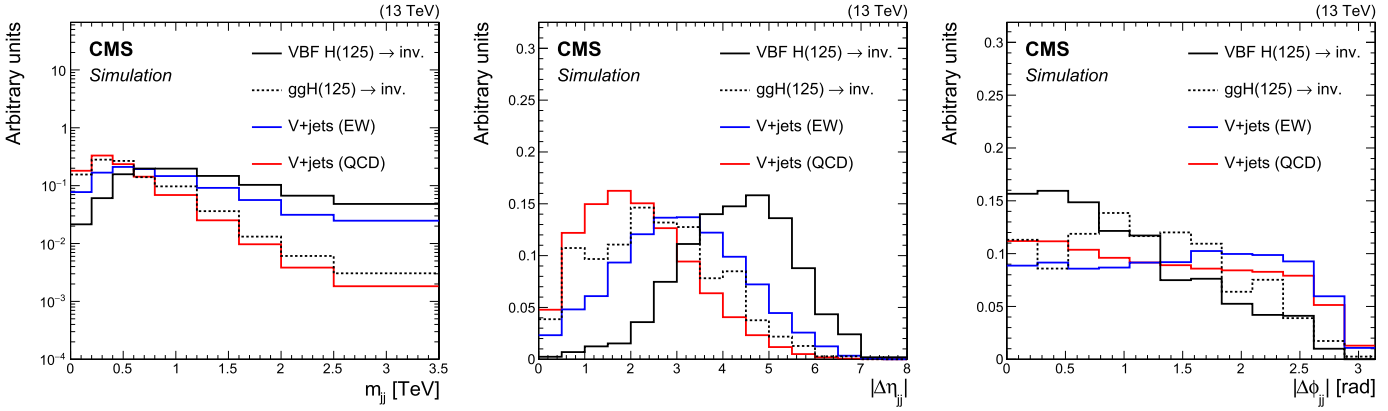

Fig. 3. Comparison between the shapes of the m_{jj} (left), $|\Delta\eta_{jj}|$ (middle) and $|\Delta\phi_{jj}|$ (right) distributions of signal events, produced by VBF (solid black) and ggH (dashed black) mechanisms, and V+jets backgrounds from both QCD (solid red) and EW (solid blue) production. Both signal and background distributions are scaled in order to have unit area. Distributions are obtained from simulated events passed through the CMS event reconstruction.

CR consisting mostly of Z($\ell\ell$)+jets events that are kinematically similar to Z($\nu\overline{\nu}$)+jets background if the presence of the two leptons in the event is ignored. The W+jets background is estimated using CRs consisting of single-muon and single-electron events stemming mainly from leptonic decays of a W boson. In contrast to the W+jets background in the SR, the single-lepton CRs consist of leptons that fall within the detector acceptance and pass the identification requirements. The $p_{\mathrm{T}}^{\mathrm{miss}}$ in all the CRs is calculated by excluding the contribution of the identified leptons. Therefore, it corresponds to the p_{T} of the hadronic recoil system, which resembles the $p_{\mathrm{T}}^{\mathrm{miss}}$ expected from the V+jets backgrounds in the SR.

The event yield in the dilepton CRs is considerably smaller than the Z($\nu\overline{\nu}$)+jets contribution in the SR because the Z($\ell\ell$) branching fraction, where $\ell = \mu$ or e, is six times smaller than the Z($\nu\overline{\nu}$) branching fraction. Consequently, the dilepton CRs have a limited statistical power to constrain the Z($\nu\overline{\nu}$)+jets background by themselves. In contrast, the yield of the single-lepton CRs is comparable to the Z($\nu\overline{\nu}$)+jets background. Furthermore, the Z($\nu\overline{\nu}$)+jets and W($\ell\nu$)+jets processes are kinematically similar if the presence of the charged lepton is ignored. The theoretical uncertainties involved in the prediction of the Z+jets and W+jets cross sections largely cancel out in their ratio. Therefore, this ratio is predicted very reliably by the simulation and can be used as a constraint to connect the statistically rich single-lepton CRs to the Z($\nu\overline{\nu}$)+jets background in the SR.

The predictions for the V+jets processes obtained from simulation are referred to as "pre-fit" expectations, and are considered to be the initial estimates for the V+jets yields in the CRs and SR. These V+jets yields are then treated as freely floating parameters, and are fit to the data in all CRs and the SR. The V+jets yields obtained from this fit are referred to as "post-fit" estimates, and serve as the final V+jets background predictions in the analysis.

6.2. Definition of control regions

Dimuon and single-muon CRs are selected using the same L1 and HLT $p_{\mathrm{T}}^{\mathrm{miss}}$-based triggers that are used to collect events in the SR. Dimuon events are required to contain exactly two oppositely charged muons with $p_{\mathrm{T}} > 10\,\mathrm{GeV}$ that form an invariant mass ($m_{\mu\mu}$) between 60 and 120 GeV, which is compatible with a Z boson decay. Events with additional electrons or photons are rejected. At least one of the two muons must have $p_{\mathrm{T}} > 20\,\mathrm{GeV}$, and is required to pass tighter identification criteria based on the number of measurements in the tracker and the muon systems, the quality of the muon track fit, and the consistency of the muon track with the primary vertex. The isolation, as defined in Section 3, is required to be smaller than 15% of the muon p_{T}. These tightly identified muons are selected with an average efficiency of 90%.

In the single-muon CR, events are required to contain exactly one muon with $p_{\mathrm{T}} > 20\,\mathrm{GeV}$, passing both tight identification and isolation requirements. The transverse mass (m_{T}) of the muon-$p_{\mathrm{T}}^{\mathrm{miss}}$ system is computed as $m_{\mathrm{T}} = \sqrt{2 p_{\mathrm{T}}^{\mathrm{miss}} p_{\mathrm{T}}^{\mu} (1 - \cos\Delta\phi)}$, where p_{T}^{μ} is the p_{T} of the muon, and $\Delta\phi$ is the angle between $\vec{p}_{\mathrm{T}}^{\,\mu}$ and $\vec{p}_{\mathrm{T}}^{\,\mathrm{miss}}$ in the transverse plane. The m_{T} is required to be smaller than 160 GeV, and no additional electrons or photons are allowed in the event.

Events in the dielectron and single-electron CRs are collected mainly using a single-electron trigger with a p_{T} threshold of

27 GeV. In the case of dielectron events where the Z boson has $p_T > 600$ GeV, the two electrons have a small angular separation, and are likely to get included in each other's isolation cones. This results in an inefficiency for the chosen trigger that imposes isolation requirements on electron candidates. This inefficiency is mitigated by including events collected by a single-electron trigger with a p_T threshold of 105 GeV and no isolation requirements on the electron candidate.

The dielectron events are required to contain exactly two oppositely charged electrons with $p_T > 10$ GeV and no additional muons or photons. As in the case of the dimuon events, the invariant mass of the dielectron system is required to be between 60 and 120 GeV. At least one of the two electrons must have $p_T > 40$ GeV, and is required to pass a tight identification criterion based on the shower shape of its ECAL energy deposit, the matching of the electron track to the ECAL energy cluster, and the consistency of the electron track with the primary vertex. Furthermore, the isolation is required to be smaller than 6% of the electron p_T. These selection requirements for electrons have an average efficiency of 70%.

Events in the single-electron CR are required to contain exactly one tightly identified and isolated electron with $p_T > 40$ GeV; no additional muons or photons are allowed. The contamination from QCD multijet events is reduced by requiring $p_T^{miss} > 60$ GeV and $m_T < 160$ GeV.

Events in the CRs must also satisfy the requirements imposed on events in the SR. When doing so, the negative p_T of the hadronic recoil system is used instead of the p_T^{miss} in the event.

6.3. Estimation of V+jets backgrounds

The V+jets yields in the CRs are translated to the background estimates in the SR using transfer factors that are derived from simulation. The transfer factors are defined as the ratio of the yields of a given V+jets background in the SR and the corresponding process measured in each CR.

The transfer factors for the dilepton CRs account for the difference in the branching fractions of the $Z(\nu\overline{\nu})$ and $Z(\ell\ell)$ decays, and the $\gamma^*(\ell\ell)$ contribution, as well as the impact of lepton acceptance and selection efficiencies. In the case of dielectron events, the transfer factors also account for the difference in trigger efficiencies. Transfer factors between the $W(\ell\nu)$+jets event yields in the single-lepton CRs and the W+jets background estimate in the SR take into account the effect of lepton acceptance, selection efficiencies, and lepton and τ_h veto efficiencies, as well as the difference in trigger efficiencies in the case of the single-electron CR.

The constraint on the ratio of the cross sections of the Z+jets and W+jets processes, which is used to connect the single-lepton CRs to the $Z(\nu\overline{\nu})$+jets in the SR, is also implemented as a transfer factor, and is computed as the ratio of the $Z(\nu\overline{\nu})$+jets and $W(\ell\nu)$+jets yields in the SR. In order to have the most precise estimate of this constraint, the LO simulations for the Z+jets (QCD) and the W+jets (QCD) processes are corrected using boson p_T and m_{jj}–dependent NLO QCD K-factors derived with MadGraph5_aMC@NLO. The Z+jets and W+jets simulations are also corrected as a function of boson p_T with NLO EW K-factors derived from theoretical calculations [53]. Similarly, Z+jets (EW) and W+jets (EW) processes are corrected with NLO QCD K-factors derived using the VBFNLO event generator [54,55] as a function of boson p_T and m_{jj}.

The V+jets background yields are determined using a maximum-likelihood fit, performed simultaneously across all CRs and the SR. The likelihood function is defined as:

$$
\begin{aligned}
&\mathcal{L}(\mu, \kappa^{\nu\overline{\nu}}, \boldsymbol{\theta}) = \\
&\prod_i \mathrm{P}\Bigg(d_i \Big| B_i(\boldsymbol{\theta}) + (1 + f_i(\boldsymbol{\theta})_{\mathrm{Q}})\kappa_i{}^{\nu\overline{\nu}} \\
&\qquad + R_i^{\mathrm{Z}}(1 + f_i(\boldsymbol{\theta})_{\mathrm{E}})\kappa_i{}^{\nu\overline{\nu}} + \mu S_i(\boldsymbol{\theta})\Bigg) \\
&\prod_i \mathrm{P}\left(d_i^{\mu\mu} \Big| B_i^{\mu\mu}(\boldsymbol{\theta}) + \frac{\kappa_i{}^{\nu\overline{\nu}}}{R_i^{\mu\mu}(\boldsymbol{\theta})_{\mathrm{Q}}} + \frac{R_i^{\mathrm{Z}}\kappa_i{}^{\nu\overline{\nu}}}{R_i^{\mu\mu}(\boldsymbol{\theta})_{\mathrm{E}}}\right) \\
&\prod_i \mathrm{P}\left(d_i^{\mathrm{ee}} \Big| B_i^{\mathrm{ee}}(\boldsymbol{\theta}) + \frac{\kappa_i{}^{\nu\overline{\nu}}}{R_i^{\mathrm{ee}}(\boldsymbol{\theta})_{\mathrm{Q}}} + \frac{R_i^{\mathrm{Z}}\kappa_i{}^{\nu\overline{\nu}}}{R_i^{\mathrm{ee}}(\boldsymbol{\theta})_{\mathrm{E}}}\right) \\
&\prod_i \mathrm{P}\left(d_i^{\mu} \Big| B_i^{\mu}(\boldsymbol{\theta}) + \frac{f_i(\boldsymbol{\theta})_{\mathrm{Q}}\kappa_i{}^{\nu\overline{\nu}}}{R_i^{\mu}(\boldsymbol{\theta})_{\mathrm{Q}}} + \frac{R_i^{\mathrm{Z}} f_i(\boldsymbol{\theta})_{\mathrm{E}}\kappa_i{}^{\nu\overline{\nu}}}{R_i^{\mu}(\boldsymbol{\theta})_{\mathrm{E}}}\right) \\
&\prod_i \mathrm{P}\left(d_i^{\mathrm{e}} \Big| B_i^{\mathrm{e}}(\boldsymbol{\theta}) + \frac{f_i(\boldsymbol{\theta})_{\mathrm{Q}}\kappa_i{}^{\nu\overline{\nu}}}{R_i^{\mathrm{e}}(\boldsymbol{\theta})_{\mathrm{Q}}} + \frac{R_i^{\mathrm{Z}} f_i(\boldsymbol{\theta})_{\mathrm{E}}\kappa_i{}^{\nu\overline{\nu}}}{R_i^{\mathrm{e}}(\boldsymbol{\theta})_{\mathrm{E}}}\right) \prod_j \mathrm{P}(\theta)
\end{aligned}
\tag{1}
$$

where $\mathrm{P}(x|y) = y^x \mathrm{e}^{-y}/x!$. The symbol i denotes each bin of the m_{jj} distribution in the shape analysis, while, in the cut-and-count case, i stands for a single bin that represents the event yields obtained at the end of the event selection. The symbols $d_i^{\mu\mu}$, d_i^{ee}, d_i^{μ}, d_i^{e}, and d_i denote the observed number of events in each bin i of the dimuon, dielectron, single-muon, single-electron CRs, and the SR, respectively. The symbols $f_i(\boldsymbol{\theta})_{\mathrm{Q}}$ and $f_i(\boldsymbol{\theta})_{\mathrm{E}}$ indicate the ratios between the $W(\ell\nu)$+jets and $Z(\nu\overline{\nu})$+jets backgrounds in the SR from QCD and EW production, respectively. The symbols $R_i^{\mu\mu}(\boldsymbol{\theta})_{\mathrm{Q}}$, $R_i^{\mathrm{ee}}(\boldsymbol{\theta})_{\mathrm{Q}}$, $R_i^{\mu}(\boldsymbol{\theta})_{\mathrm{Q}}$, and $R_i^{\mathrm{e}}(\boldsymbol{\theta})_{\mathrm{Q}}$ are the transfer factors relating the dimuon, dielectron, single-muon, and single-electron CRs, respectively, to the SR for the V+jets (QCD) processes. Similarly, $R_i^{\mu\mu}(\boldsymbol{\theta})_{\mathrm{E}}$, $R_i^{\mathrm{ee}}(\boldsymbol{\theta})_{\mathrm{E}}$, $R_i^{\mu}(\boldsymbol{\theta})_{\mathrm{E}}$, and $R_i^{\mathrm{e}}(\boldsymbol{\theta})_{\mathrm{E}}$ indicate the transfer factors for the V+jets (EW) processes. The parameters $\kappa_i{}^{\nu\overline{\nu}}$ represent the yield of the $Z(\nu\overline{\nu})$+jets (QCD) background in each bin i of the SR, and are left to float freely in the fit. In a given bin, the $Z(\nu\overline{\nu})$+jets (EW) background yield is obtained from $\kappa_i{}^{\nu\overline{\nu}}$ through the transfer factor R_i^{Z} that represents the ratio between the $Z(\nu\overline{\nu})$+jets (QCD) and $Z(\nu\overline{\nu})$+jets (EW) processes. The contributions from subleading backgrounds in each region are estimated directly from simulation and they are denoted by $B_i^{\mu\mu}$, B_i^{ee}, B_i^{μ}, B_i^{e} and B_i. Finally, the likelihood also includes a signal term in which S_i represents the expected signal prediction, while $\mu = (\sigma/\sigma_{\mathrm{SM}})\,\mathcal{B}(\mathrm{H} \to \mathrm{inv})$ denotes the signal strength parameter.

Systematic uncertainties are modeled as constrained nuisance parameters ($\boldsymbol{\theta}$), for which log-normal or Gaussian priors, indicated by $\mathrm{P}_j(\theta)$ in previous equation, are considered. The systematic uncertainties in the V+jets background estimates are introduced in the likelihood as variations of the transfer factors. These include theoretical uncertainties in the Z+jets to W+jets differential cross section ratio for both the QCD and EW processes due to the choice of the renormalization and the factorization scales, as well as the choice of the PDFs. The QCD scale variations are assumed to be uncorrelated between the Z+jets and W+jets processes, and therefore they do not cancel in the Z+jets to W+jets cross section ratio. This results in larger uncertainties compared to those from NLO calculations recommended in Ref. [53]. The uncertainty due to the choice of the renormalization scale varies between 8 and 12% as a function of m_{jj} for both Z+jets/W+jets (QCD) and (EW) ratios. Similarly, the uncertainty due to the choice of the factorization scale varies between 2 and 7%. This also covers the uncertainty in the Z+jets/W+jets cross section ratio due to the interference between the V+jets (QCD) and V+jets (EW) processes, which is not included in the simulation. The PDF uncertainties are assumed to

Table 2
Experimental and theoretical sources of systematic uncertainties on the V+jets transfer factors, which enter in the simultaneous fit, used to estimate the V+jets backgrounds, as constrained nuisance parameters. In addition, the impact on the fitted signal strength, $(\sigma/\sigma_{SM})\,\mathcal{B}(H \to \text{inv})$, is reported in the last column estimated after performing the m_{jj} shape fit to the observed data across signal and control regions.

Source of uncertainty	Ratios	Uncertainty vs. m_{jj}	Impact on $\mathcal{B}(H \to \text{inv})$
Theoretical uncertainties			
Ren. scale V+jets (EW)	$Z(\nu\overline{\nu})/W(\ell\nu)$ (EW)	9–12%	48%
Ren. scale V+jets (QCD)	$Z(\nu\overline{\nu})/W(\ell\nu)$ (QCD)	9–12%	25%
Fac. scale V+jets (EW)	$Z(\nu\overline{\nu})/W(\ell\nu)$ (EW)	2–7%	4%
Fac. scale V+jets (QCD)	$Z(\nu\overline{\nu})/W(\ell\nu)$ (QCD)	2–7%	2%
PDF V+jets (QCD)	$Z(\nu\overline{\nu})/W(\ell\nu)$ (QCD)	0.5–1%	<1%
PDF V+jets (EW)	$Z(\nu\overline{\nu})/W(\ell\nu)$ (EW)	0.5–1%	<1%
NLO EW corr.	$Z(\nu\overline{\nu})/W(\ell\nu)$ (QCD)	1–2%	<1%
Experimental uncertainties			
Muon reco. eff.	$Z(\mu\mu)/Z(\nu\overline{\nu})$, $W(\mu\nu)/W(\ell\nu)$	≈1% (per lepton)	8%
Electron reco. eff.	$Z(ee)/Z(\nu\overline{\nu})$, $W(e\nu)/W(\ell\nu)$	≈1% (per lepton)	3%
Muon id. eff.	$Z(\mu\mu)/Z(\nu\overline{\nu})$, $W(\mu\nu)/W(\ell\nu)$	≈1% (per lepton)	8%
Electron id. eff.	$Z(ee)/Z(\nu\overline{\nu})$, $W(e\nu)/W(\ell\nu)$	≈1.5% (per lepton)	4%
Muon veto	$Z(\nu\overline{\nu})/W(\ell\nu)$, W(CRs)/$W(\ell\nu)$	≈2.5 (2)% for EW (QCD)	7%
Electron veto	$Z(\nu\overline{\nu})/W(\ell\nu)$, W(CRs)/$W(\ell\nu)$	≈1.5 (1)% for EW (QCD)	5%
τ veto	$Z(\nu\overline{\nu})/W(\ell\nu)$, W(CRs)/$W(\ell\nu)$	≈3.5 (3)% for EW (QCD)	13%
Jet energy scale	Z(CRs)/$Z(\nu\overline{\nu})$, W(CRs)/$W(\ell\nu)$	≈1 (2)% for Z/Z (W/W)	4%
Electron trigger	$Z(ee)/Z(\nu\overline{\nu})$, $W(e\nu)/W(\ell\nu)$	≈1%	<1%
p_T^{miss} trigger	All ratios	≈2%	18%

be correlated across V+jets processes, resulting in a residual uncertainty smaller than 1% on the Z+jets/W+jets cross section ratio. The uncertainties related to NLO EW corrections to the V+jets (QCD) processes are estimated according to the recommendations in Ref. [53], and are found to be about 1–2% across the entire m_{jj} spectrum. Additional uncertainties included in the transfer factors include uncertainties in the reconstruction efficiencies of leptons (around 1% per muon or electron), the selection efficiencies of leptons (about 1% per muon, 1.5% per electron), the veto efficiency of leptons (around 2% per muon, 1% per electron) and τ_h candidates (about 3.5% per τ_h), the knowledge of the jet energy scale (1–2%), and the efficiency of the electron (around 1%) and p_T^{miss} triggers (about 2%).

The full set of systematic uncertainties related to the V+jets transfer factors are listed in Table 2. Before any fit is performed, the total uncertainty in the expected background in the SR ranges between 4.5 and 6% as a function of m_{jj}, dominated by the theoretical uncertainties in the Z+jets to W+jets cross section ratio for both QCD and EW production. The impact of each source of systematic uncertainty, as reported in Table 2 in the context of the shape analysis, is defined as the maximum difference in the fitted value of the signal strength, $(\sigma/\sigma_{SM})\,\mathcal{B}(H \to \text{inv})$, obtained by varying the associated nuisance parameter within one standard deviation of its maximum likelihood estimate. In this procedure, the per-bin $\kappa_i{}^{\nu\overline{\nu}}$ parameters are profiled when a given nuisance parameter is shifted from its best fit estimate.

The m_{jj} distributions in the dilepton and single-lepton CRs are shown in Fig. 4. The pre-fit predictions for the V+jets processes are shown in red. These indicate the level of agreement between data and simulation before a fit is performed. An estimate of the V+jets backgrounds is then obtained by fitting the data across all the CRs. This is depicted by the blue line in Fig. 4. This fit is referred to as the "CR-only" fit, since it does not impose any constraint on the V+jets yields due to the data in the SR.

To assess the level of agreement between data and simulation obtained through the application of p_T–m_{jj} dependent NLO corrections to both the V+jets (QCD) and V+jets (EW) processes, the ratio between the number of Z+jets and W+jets events in the CRs in bins of m_{jj} is used as a benchmark. Fig. 5 shows the ratio of the Z+jets and W+jets event yields in the muon (left) and electron (right) CRs, respectively. A good agreement is observed between data and simulation and local differences are covered by the systematic uncertainties listed in Table 2.

6.4. Other backgrounds

In addition to the V+jets processes, several other minor sources of background contribute to the total event yield in the SR. These include QCD multijet events that typically have small genuine p_T^{miss}. However, jet momentum mismeasurements and instrumental effects may give rise to large p_T^{miss} tails. A min$\Delta\phi$ extrapolation method [56] is used to estimate this background from data, where a QCD multijet enriched CR is defined by selecting events that fail the min$\Delta\phi$ requirement between the jets and the $\vec{p}_T^{miss}$ vector, but still fulfill the remaining event selection criteria. A transfer factor, derived from simulated QCD multijet events, is used to estimate the background in the SR from the event rate measured in the low-$\Delta\phi(\vec{p}_T^{miss}, \vec{p}_T^{jet})$ sample. The low-$\Delta\phi(\vec{p}_T^{miss}, \vec{p}_T^{jet})$ region contains a significant contamination from V+jets production, which have genuine p_T^{miss}. They contribute about 40% of the total event yield for m_{jj} smaller than 500 GeV, and about 80% for $m_{jj} > 3$ TeV. This contamination is estimated from simulation and subtracted from the event yield measured in the low-$\Delta\phi(\vec{p}_T^{miss}, \vec{p}_T^{jet})$ sample. An uncertainty of 20% is assigned while performing the subtraction, which results in an uncertainty of about 30% in the estimated QCD multijet background in the SR. The MC statistical uncertainty of the QCD multijet samples, which affects the transfer factor prediction, is also considered and is found to vary between 40 and 100% as a function of m_{jj}. Lastly, a validation of the $\Delta\phi$ method is performed using a purer sample of QCD multijet events that pass the analysis requirements, but have p_T^{miss} in the range of 100–175 GeV. In this validation region, the predicted QCD background is found to agree with the observation within 50%, which is taken as a conservative estimate of an additional uncertainty.

The remaining background sources include top quark production and diboson processes, which are estimated from simulation. The p_T distribution of the top quark in simulation is corrected to match the observed p_T distribution in data [57]. An uncertainty of about 10% is assigned to the overall top quark background normalization, while an additional 10% uncertainty is added to account for the modeling of the top quark p_T distribution in simulation. The overall normalization of the diboson background has an un-

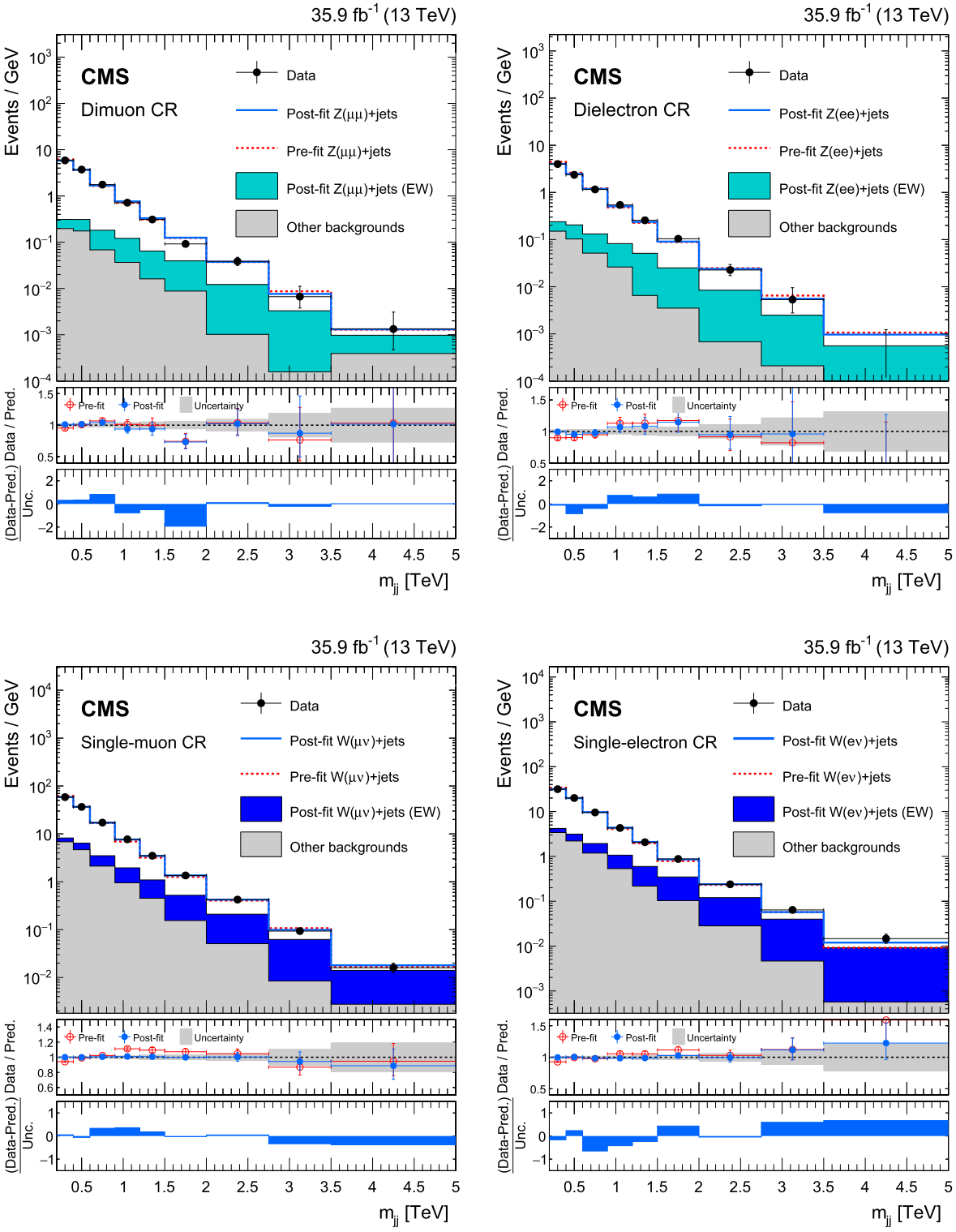

Fig. 4. The m_{jj} distributions in the dimuon (top left), dielectron (top right), single-muon (bottom left), and single-electron (bottom right) CRs as computed in the shape analysis. Prediction from simulation (pre-fit estimate) is shown by the dashed red line. The solid blue line shows the V+jets expectation after fitting the data in all the CRs. The filled histograms indicate all processes other than V+jets (QCD). The last bin includes all events with $m_{jj} > 3.5$ TeV. Ratios of data and the pre-fit background (red points) and the post-fit background prediction (blue points) are shown. The gray band in the ratio panel indicates the total uncertainty after performing the fit. The lowest panel shows the difference between data and the post-fit background estimate relative to the post-fit background uncertainty.

certainty of about 15% [58,59]. The uncertainties in the top quark and diboson backgrounds are correlated across the SR and the CRs. Several experimental sources of uncertainty are also assigned to these backgrounds. An uncertainty of 2.5% in the integrated luminosity measurement [60] is propagated to the background yields. The uncertainty in the efficiency of the b quark jet veto is estimated to be around 3% for the top quark background and of about 1% for the other simulated processes. The uncertainty related to

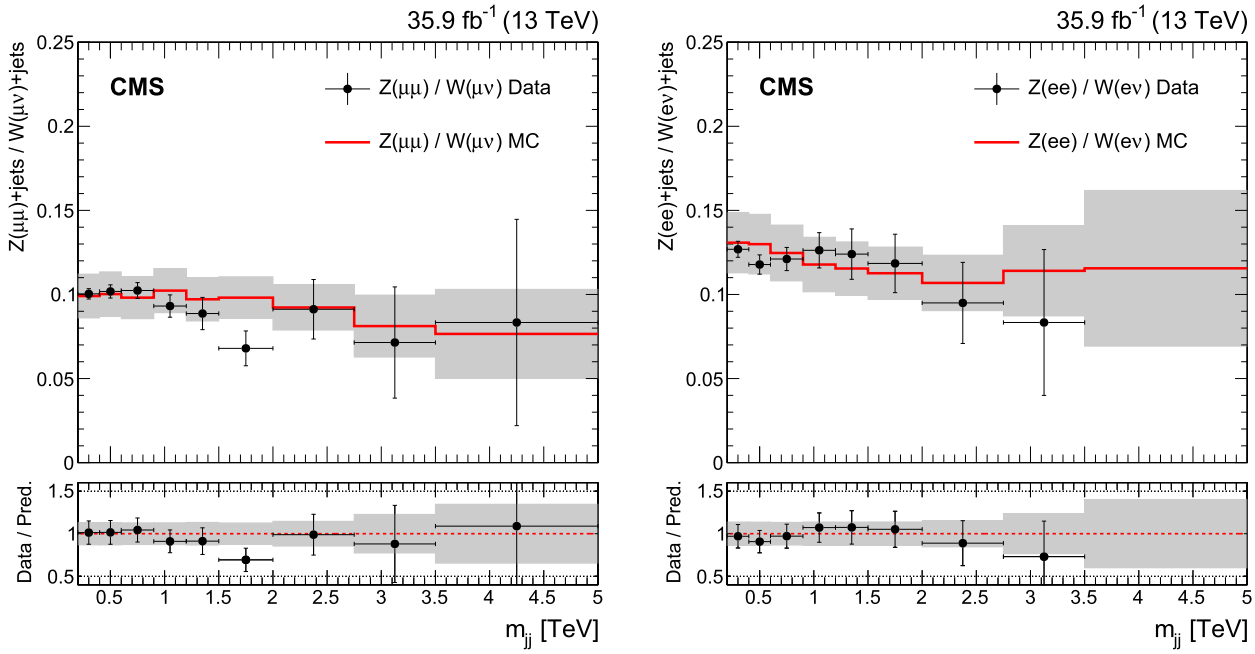

Fig. 5. Comparison between data and simulation of the Z($\mu\mu$)+jets/W($\mu\nu$)+jets (left) and Z(ee)+jets/W(eν)+jets (right) ratios as functions of m_{jj}, computed in the shape analysis phase-space. In the bottom panels, ratios of data with the pre-fit background prediction are reported. The gray bands include both the theoretical and experimental systematic uncertainties listed in Table 2, as well as the statistical uncertainty in the simulation.

the jet energy scale varies between 8 and 15%, depending on both the process and the CR.

7. Results

This section presents the results obtained from the shape and the cut-and-count analyses. These include 95% CL upper limits on $\mathcal{B}(\mathrm{H} \to \mathrm{inv})$, and an interpretation of the search in the context of a BSM model which allows for the presence of a SM-like Higgs boson with a mass between 110 and 1000 GeV.

7.1. The shape analysis

The observed and the expected m_{jj} distributions in the SR, obtained after applying the full event selection, are shown in Fig. 6. The background prediction shown in Fig. 6 (left) is obtained from a fit to the data in the CRs. Signal distributions for the SM Higgs boson produced via the ggH and VBF modes are overlaid, assuming $\mathcal{B}(\mathrm{H} \to \mathrm{inv}) = 1$. The estimated background yields from the CR-only fit are listed in Table 3, along with the observed event yield in the SR. The large contamination from ggH production arises from the low-m_{jj} bins, which represent the least sensitive region to H → inv decays. Systematic uncertainties in the V+jets transfer factors and in the minor backgrounds introduce correlations across the m_{jj} bins used in the fit. The correlations in the predicted background yields in each m_{jj} bin are reported in Table 4.

An excess of about 4–10% is observed in the SR data when compared to the estimated backgrounds. The discrepancy resides mainly in the bulk of the m_{jj} distribution. The shape of the excess is inconsistent with the characteristic features of a VBF signal, whose presence is expected to produce an increasing discrepancy between data and backgrounds as m_{jj} increases. A goodness of fit test, based on a saturated χ^2 test statistic [61,62], yields a p-value of about 6% indicating that the data are compatible with the SM prediction.

Fig. 6 (right) shows the background prediction obtained after including events from the SR in the fit, but assuming the absence of a signal. Such a fit is referred to as the "b-only fit". The comparison between the results of the b-only fit with that allowing for the presence of the signal is used to set an upper limit on $\mathcal{B}(\mathrm{H} \to \mathrm{inv})$. In the b-only fit, the V+jets estimate in the SR can vary with respect to the prediction from the CRs within the systematic uncertainties assigned to the transfer factors. Therefore, the additional constraint due to the data in the SR mitigates the excess shown in Fig. 6 (left), yielding a p-value for the b-only fit of about 65%.

The results of this search are interpreted in terms of an upper limit on the product of the Higgs boson production cross section and its branching fraction to invisible particles, $\sigma\mathcal{B}(\mathrm{H} \to \mathrm{inv})$, relative to the predicted cross section assuming SM interactions, σ_{SM}. Observed and expected 95% CL upper limits are computed using an asymptotic approximation of the $\mathrm{CL_s}$ method [63,64] with a profile likelihood ratio test statistic [65] in which systematic uncertainties are modeled as nuisance parameters following a frequentist approach [66]. The profile likelihood ratio is defined as:

$$q = -2\Delta \ln \mathcal{L} = -2 \ln \frac{\mathcal{L}(\mathrm{data}|(\sigma/\sigma_{\mathrm{SM}})\,\mathcal{B}(\mathrm{H} \to \mathrm{inv}), \hat{\boldsymbol{\theta}}_{\boldsymbol{a}}, \hat{\boldsymbol{\kappa}}_{\boldsymbol{a}})}{\mathcal{L}(\mathrm{data}|(\sigma/\sigma_{\mathrm{SM}})\,\hat{\mathcal{B}}(\mathrm{H} \to \mathrm{inv}), \hat{\boldsymbol{\theta}}, \hat{\boldsymbol{\kappa}})} \quad (2)$$

where $(\sigma/\sigma_{\mathrm{SM}})\,\hat{\mathcal{B}}(\mathrm{H} \to \mathrm{inv})$ represents the value of the signal strength that maximizes the likelihood $\mathcal{L}$ for the data, while $\hat{\boldsymbol{\theta}}$ ($\hat{\boldsymbol{\kappa}}$) and $\hat{\boldsymbol{\theta}}_{\boldsymbol{a}}$ ($\hat{\boldsymbol{\kappa}}_{\boldsymbol{a}}$) denote the best fit estimates for the nuisance parameters (Z($\nu\overline{\nu}$)+jets rate in each bin) and the estimates for a given fixed value of $(\sigma/\sigma_{\mathrm{SM}})\,\mathcal{B}(\mathrm{H} \to \mathrm{inv})$, respectively.

The relative contributions of the VBF and ggH production modes are fixed to the SM prediction within their uncertainties. The uncertainties in the predictions of the inclusive VBF and ggH production cross sections due to PDF uncertainties, renormalization and factorization scale variations are taken from Ref. [34]. An additional uncertainty of 40% is assigned to the expected ggH contribution. This accounts for both the limited knowledge of the ggH cross section in association with two or more jets, as well as the

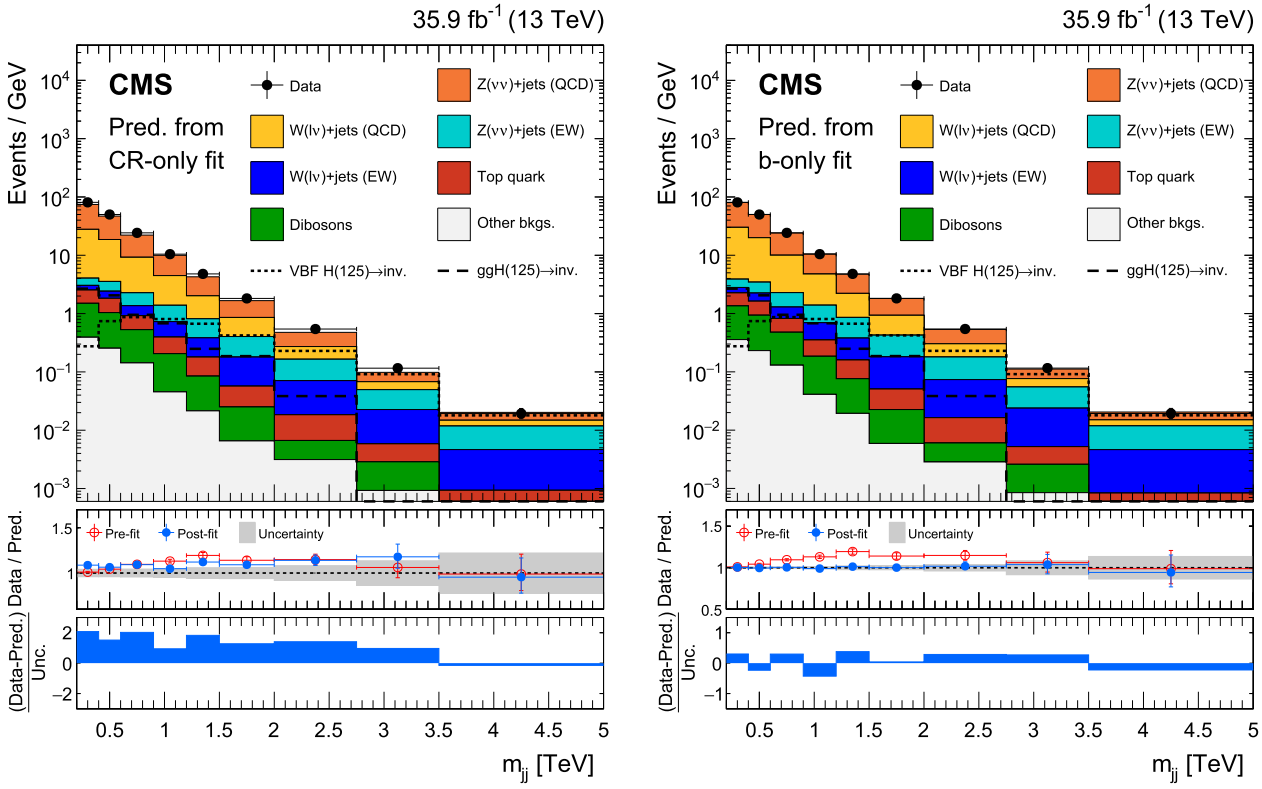

Fig. 6. The observed m_{jj} distribution of the shape analysis SR compared to the post-fit backgrounds from various SM processes. On the left, the predicted backgrounds are obtained from a combined fit to the data in all the CRs, but excluding the SR. On the right, the predicted backgrounds are obtained from a combined fit to the data in all the CRs, as well as in the SR, assuming the absence of any signal. Expected signal distributions for a 125 GeV Higgs boson produced through ggH and VBF modes, and decaying to invisible particles with a branching fraction $\mathcal{B}(\mathrm{H} \to \mathrm{inv}) = 1$, are overlaid. The last bin includes all events with $m_{jj} > 3.5$ TeV. The description of the ratio panels is the same as in Fig. 4.

Table 3
Expected event yields in each m_{jj} bin for various background processes in the SR of the shape analysis. The background yields and the corresponding uncertainties are obtained after performing a combined fit across all the CRs, but excluding data in the SR. The "other backgrounds" includes QCD multijet and Z($\ell\ell$)+jets processes. The expected total signal contribution for the 125 GeV Higgs boson, decaying to invisible particles with a branching fraction $\mathcal{B}(\mathrm{H} \to \mathrm{inv}) = 1$, and the observed event yields are also reported.

Process	m_{jj} range in TeV								
	0.2–0.4	0.4–0.6	0.6–0.9	0.9–1.2	1.2–1.5	1.5–2.0	2.0–2.75	2.75–3.5	>3.5
Z($\nu\nu$) (QCD)	9311 ± 388	5669 ± 257	3884 ± 179	1648 ± 88	677 ± 42	405 ± 28	153 ± 14	22.8 ± 3.5	8.1 ± 2.2
Z($\nu\nu$) (EW)	201 ± 8	228 ± 10	273 ± 13	198 ± 11	129 ± 8	112 ± 8	70.6 ± 6.6	20.2 ± 3.1	10.8 ± 2.9
W($\ell\nu$) (QCD)	4755 ± 267	3017 ± 180	2090 ± 130	928 ± 63	361 ± 28	227 ± 19	80.4 ± 9.1	13.7 ± 2.7	4.5 ± 1.9
W($\ell\nu$) (EW)	102 ± 14	118 ± 16	133 ± 18	100 ± 13	61.2 ± 8.1	61.4 ± 7.6	39.4 ± 4.9	12.6 ± 1.9	5.6 ± 1.4
Top quark	208 ± 37	159 ± 28	119 ± 21	57.6 ± 10.2	28.7 ± 5.1	16.1 ± 2.9	8.9 ± 1.6	2.2 ± 0.4	0.7 ± 0.1
Dibosons	222 ± 39	157 ± 28	116 ± 21	48.2 ± 8.5	19.0 ± 3.4	9.3 ± 1.6	2.6 ± 0.5	1.4 ± 0.3	0.4 ± 0.1
Others	78.6 ± 19.5	51.0 ± 11.6	42.8 ± 11.5	13.6 ± 2.9	6.5 ± 1.5	3.3 ± 0.8	2.4 ± 0.6	0.7 ± 0.2	0.3 ± 0.4
Total bkg.	14878 ± 566	9401 ± 387	6658 ± 271	2994 ± 144	1283 ± 69	834 ± 51	358 ± 29	73.8 ± 9.4	30.3 ± 7.4
Signal	590 ± 244	559 ± 199	547 ± 151	447 ± 109	276 ± 58	304 ± 66	201 ± 36	68.6 ± 11.7	30.0 ± 6.4
Data	16177	10008	7277	3138	1439	911	408	87	29

uncertainty in the prediction of the ggH differential cross section for large Higgs boson transverse momentum, $p_{\mathrm{T}}^{\mathrm{H}} > 250$ GeV. The former contribution is obtained by following the recipe outlined in Ref. [34] and is found to be about 30%, while the latter uncertainty is estimated by comparing the prediction from POWHEG+MINLO [67] with the one from MADGRAPH5_aMC@NLO and ranges between 20 and 25%. Furthermore, the uncertainties in the signal acceptance due to the choice of the PDF set are also evaluated independently for the different signal processes, and are treated as independent nuisance parameters in the fit.

The observed (expected) 95% CL upper limit on $\mathcal{B}(\mathrm{H} \to \mathrm{inv})$ is measured to be 0.33 (0.25), and the regions containing 68% and 95% of the distribution of upper limits, expected in absence of a signal, are found to be 0.18–0.35 and 0.14–0.47, respectively.

The background estimates reported in Table 3, along with the correlation matrix presented in Table 4, can be used in the simplified likelihood approach detailed in Ref. [68] to reinterpret these results in theoretical models different from those presented in this Letter.

7.2. The cut-and-count analysis

The cut-and-count analysis is presented because it allows for an easier reinterpretation of this search in the context of other theoretical models that predict $p_{\mathrm{T}}^{\mathrm{miss}}$ plus VBF dijet signatures. The ob-

Table 4
Correlation between the uncertainties in predicted background yields across the m_{jj} bins of the shape analysis SR. The backgrounds are estimated by fitting the data in the CRs. Bin ranges are expressed in TeV.

	Correlation coefficients								
	0.2–0.4	0.4–0.6	0.6–0.9	0.9–1.2	1.2–1.5	1.5–2.0	2.0–2.75	2.75–3.5	> 3.5
0.2–0.4	1.00	–	–	–	–	–	–	–	–
0.4–0.6	0.88	1.00	–	–	–	–	–	–	–
0.6–0.9	0.85	0.84	1.00	–	–	–	–	–	–
0.9–1.2	0.78	0.76	0.75	1.00	–	–	–	–	–
1.2–1.5	0.70	0.72	0.71	0.60	1.00	–	–	–	–
1.5–2.0	0.62	0.57	0.63	0.59	0.54	1.00	–	–	–
2.0–2.75	0.38	0.40	0.43	0.43	0.45	0.43	1.00	–	–
2.75–3.5	0.28	0.28	0.33	0.26	0.34	0.27	0.22	1.00	–
>3.5	0.22	0.21	0.22	0.23	0.24	0.20	0.23	0.19	1.00

Table 5
Expected event yields in the SR and in the CRs of the cut-and-count analysis for various SM processes. The background yields and the corresponding uncertainties are obtained from a combined fit to data in all the CRs, but excluding data in the SR. The expected total signal contribution for the 125 GeV Higgs boson, decaying to invisible particles with a branching fraction $\mathcal{B}(\mathrm{H} \to \mathrm{inv}) = 1$, and the observed event yields are also reported.

Process	Signal region	Dimuon CR	Dielectron CR	Single-muon CR	Single-electron CR
$\mathrm{Z}(\nu\nu)$ (QCD)	810 ± 71	–	–	–	–
$\mathrm{Z}(\nu\nu)$ (EW)	269 ± 33	–	–	–	–
$\mathrm{Z}(\ell\ell)$ (QCD)	–	91.5 ± 7.6	66.5 ± 6.0	27.1 ± 1.2	5.2 ± 0.3
$\mathrm{Z}(\ell\ell)$ (EW)	–	32.5 ± 4.1	24.1 ± 3.2	5.7 ± 0.3	2.4 ± 0.2
$\mathrm{W}(\ell\nu)$ (QCD)	499 ± 33	0.2 ± 0.2	0.9 ± 0.6	907 ± 30	544 ± 21
$\mathrm{W}(\ell\nu)$ (EW)	141 ± 11	0.1 ± 0.1	–	406 ± 15	254 ± 11
Top quark	37.8 ± 8.8	4.8 ± 1.4	2.9 ± 1.0	112 ± 22	74.2 ± 13.6
Dibosons	18.6 ± 6.2	2.3 ± 1.1	0.7 ± 0.4	21.3 ± 4.4	14.4 ± 3.7
Others	3.3 ± 2.3	–	–	22.9 ± 13.9	2.1 ± 1.9
Total bkg.	1779 ± 96	131 ± 8	95.0 ± 6.3	1502 ± 34	896 ± 24
Signal $m_{\mathrm{H}} = 125.09$ GeV	743 ± 129	–	–	–	–
Data	2035	114	104	1504	902

served event yield after the cut-and-count selection is reported in Table 5, along with the predicted backgrounds in the SR. The backgrounds are estimated by fitting the data in the CRs. An excess, characterized by a significance of about 2.5 standard deviations, is observed in the SR compared to the background prediction obtained from the CRs. As for the shape analysis, this excess is mostly due to low m_{jj} events. The excess is incompatible with a VBF Higgs boson signal and, upon detailed scrutiny, is ascribed to a statistical fluctuation.

The results of the cut-and-count analysis are presented in terms of a 95% CL upper limit on $\mathcal{B}(\mathrm{H} \to \mathrm{inv})$ using the statistical procedure outlined in Section 7.1. The observed (expected) upper limit is found to be 0.58 (0.30), and the regions containing 68% and 95% of the distribution of upper limits, expected in absence of a signal, are found to be 0.22–0.43 and 0.17–0.58, respectively.

7.3. Constraints on a SM-like Higgs boson

The results presented are also interpreted in the context of an additional SM-like Higgs boson that does not mix with the 125 GeV boson and decays to invisible particles [69]. Such a boson may be produced via both the ggH and VBF mechanisms. This model has already been studied in earlier CMS publications [70–72]. Upper limits, computed at 95% CL on $(\sigma/\sigma_{\mathrm{SM}})\,\mathcal{B}(\mathrm{H} \to \mathrm{inv})$, are shown in Fig. 7 as a function of the SM-like Higgs boson mass hypothesis (m_{H}) for both the shape and the cut-and-count analyses.

8. Combined limits on H → inv from 2016 data

The common feature of all the searches included in this combination is a large $p_{\mathrm{T}}^{\mathrm{miss}}$, where at least one high-p_{T} jet or a weak boson recoils against the invisible particles produced by the Higgs boson decay. Specific topological selections are designed to reduce the contamination from large SM backgrounds, targeting a particular Higgs boson production mode. The analyses included in this combination are listed in Table 6, together with their expected signal composition and their individual upper limits on $\mathcal{B}(\mathrm{H} \to \mathrm{inv})$. The results quoted for the VBF channel come from the shape analysis described earlier in this Letter. The $\mathrm{Z}(\ell^+\ell^-)\mathrm{H}$ analysis is identical to the one described in Ref. [72], where the expected signal comes entirely from invisible decays of the SM Higgs boson produced in association with a leptonically decaying Z boson, via either $\mathrm{qq} \to \mathrm{ZH}$ or $\mathrm{gg} \to \mathrm{ZH}$ production. In contrast, the V(qq')H and the ggH-tagged searches are similar to those described in Ref. [73], but events which overlap with the VBF analysis have been removed to avoid double counting. In both the ggH and V(qq')H searches, overlapping events represent about 6(15)% of the total background for a $p_{\mathrm{T}}^{\mathrm{miss}}$ of about 250(1000) GeV. The overlap removal introduces a 5% loss in the expected exclusion sensitivity compared to that of Ref. [73]. Both the V(qq')H and the ggH searches target events with at least one high-p_{T} central jet, and their SRs contain a mixture of different production modes. This mixture results from the limited discrimination power of the substructure observables exploited to select boosted V(qq')H candidates.

No significant deviations from the SM expectations are observed in any of the searches. The results are interpreted as an upper limit on $(\sigma/\sigma_{\mathrm{SM}})\,\mathcal{B}(\mathrm{H} \to \mathrm{inv})$. These limits are calculated following the same approach described in Section 7.1. The combined likelihood fit accounts for correlations between the nuisance parameters in each search. The uncertainties in the diboson backgrounds (except for those considered in the $\mathrm{Z}(\ell\ell)\mathrm{H}$ channel), $\mathrm{t\bar{t}}$ and single top quark cross sections, lepton efficiencies, momentum scales, integrated luminosity, b quark jet and τ_{h} vetoes are correlated among all the searches. In addition, the uncertainties in the inclusive signal production cross sections, due to renormalization and factorization scale variations, and the PDF uncertainties

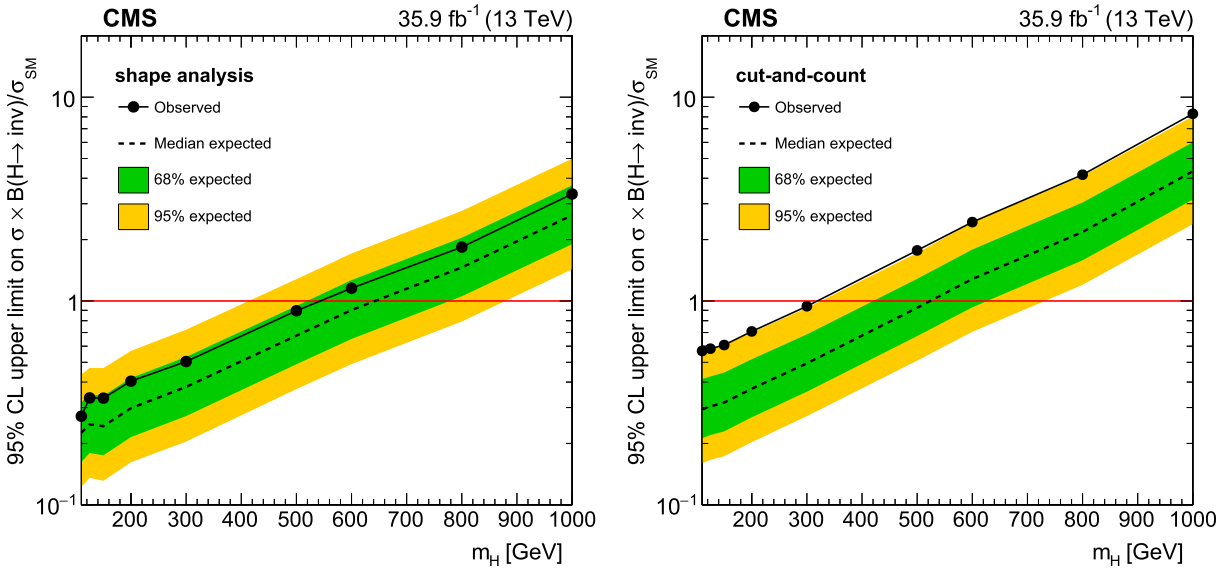

Fig. 7. Expected and observed 95% CL upper limits on $(\sigma/\sigma_{SM})\,\mathcal{B}(H \to \text{inv})$ for an SM-like Higgs boson as a function of its mass (m_H). On the left, observed (solid black) and expected (dashed black) upper limits are obtained from the shape analysis while, on the right, results from the cut-and-count analysis are reported. The 68% (green) and 95% (yellow) CL intervals around the expected upper limits are also shown for both the shape and the cut-and-count analyses.

Table 6
Signal composition and upper limits (observed and expected) on the invisible Higgs boson branching fraction classified according to the final state considered in each analysis. The relative contributions from the different Higgs production mechanisms are derived from simulation, fixing the Higgs boson mass to 125.09 GeV and assuming SM production cross sections.

Analysis	Final state	Signal composition	Observed limit	Expected limit
VBF-tag	VBF-jet + p_T^{miss}	52% VBF, 48% ggH	0.33	0.25
VH-tag	$Z(\ell\ell) + p_T^{miss}$ [72]	79% qqZH, 21% ggZH	0.40	0.42
	$V(qq') + p_T^{miss}$ [73]	39% ggH, 6% VBF, 33% WH, 22% ZH	0.50	0.48
ggH-tag	jets + p_T^{miss} [73]	80% ggH, 12% VBF, 5% WH, 3% ZH	0.66	0.59

are also correlated across the channels. In contrast, since the jet kinematics in the VBF search differ from that in the other analyses, jet energy scale and resolution uncertainties are correlated only across the ggH and VH-tagged categories. The theoretical uncertainties applied to the V+jets (QCD) ratios are assumed to be uncorrelated between the VBF analysis and the other searches.

Observed and expected upper limits on $(\sigma/\sigma_{SM})\,\mathcal{B}(H \to \text{inv})$ are computed at 95% CL and are presented in Fig. 8 (left). Assuming SM cross sections for each production mode, the combination yields an observed (expected) upper limit of $\mathcal{B}(H \to \text{inv}) < 0.26\,(0.20)$. The profile likelihood ratios as a function of $\mathcal{B}(H \to \text{inv})$, for both the combined fit and each individual search channel, are reported in Fig. 8 (right). Results are shown for both data and an Asimov dataset [65], defined by fixing the nuisances parameters to their maximum likelihood estimate obtained from a fit to the data in which $\mathcal{B}(H \to \text{inv}) = 0$ is assumed.

9. Combination of 7, 8, and 13 TeV searches for H → inv decays

The analyses previously described and listed in Table 6 are further combined with earlier searches performed using data collected at $\sqrt{s} = 7$, 8, and 13 TeV up to the end of 2015, as reported in Refs. [16,70,74]. The 7 and 8 TeV data, collected in 2011 and 2012, correspond to integrated luminosities of up to 4.9 and 19.7 fb^{-1} [75,76], respectively. The 13 TeV data collected in 2015 correspond to an integrated luminosity of 2.3 fb^{-1} [77]. Systematic uncertainties in the inclusive ggH, VBF, and VH production cross sections are fully correlated across the 7, 8, and 13 TeV analyses. The uncertainty in the prediction of the Higgs boson p_T distribution in ggH production, included in both the ggH and VH channels, and those arising from the limited knowledge of the PDFs, are also correlated among all searches. The uncertainties in the lepton and photon reconstruction and identification efficiencies, in the lepton momentum scales, and in the veto efficiency of leptons, τ_h candidates, and b quark jets are uncorrelated between 7+8 and 13 TeV searches. Similarly, uncertainties in the jet energy scale and resolution, mistag rate of leptons, and modeling of the unclustered particles are also uncorrelated between 7+8 and 13 TeV searches. The b jet energy scale and resolution uncertainties for the Z(bb)H analysis are estimated using different techniques, and therefore are treated as uncorrelated with other channels. Theoretical uncertainties affecting the ratio of $Z(\nu\overline{\nu})$ and $W(\ell\nu)$ predictions in the VBF searches, for both QCD and EW V+jets processes, are uncorrelated across data sets because different strategies are followed to quantify and assign these uncertainties. In contrast, those affecting the $Z(\nu\overline{\nu})/W(\ell\nu)$ and $Z(\nu\overline{\nu})/\gamma$+jets ratios in the ggH and V(qq)H channels are correlated across the 7+8 and the 13 TeV (2015 data) searches, as described in Ref. [16]. The uncertainties in the tune of the underlying event simulation and in the pileup modeling are uncorrelated between 7+8 and 13 TeV searches. Finally, theoretical uncertainties affecting diboson and top quark cross sections, except for those considered on the ZZ/WZ ratio in the $Z(\ell\ell)$H channel, are correlated across all data sets.

Observed and expected upper limits on $(\sigma/\sigma_{SM})\,\mathcal{B}(H \to \text{inv})$ at 95% CL are presented in Fig. 9 (left). Limits are computed for the combination of all data sets, as well as for partial combinations based either on 7+8 or 13 TeV data. The relative contributions from different Higgs production mechanisms are constrained to their SM values within the theoretical uncertainties. The combination yields an observed (expected) upper limit of $\mathcal{B}(H \to \text{inv}) < 0.19\,(0.15)$ at

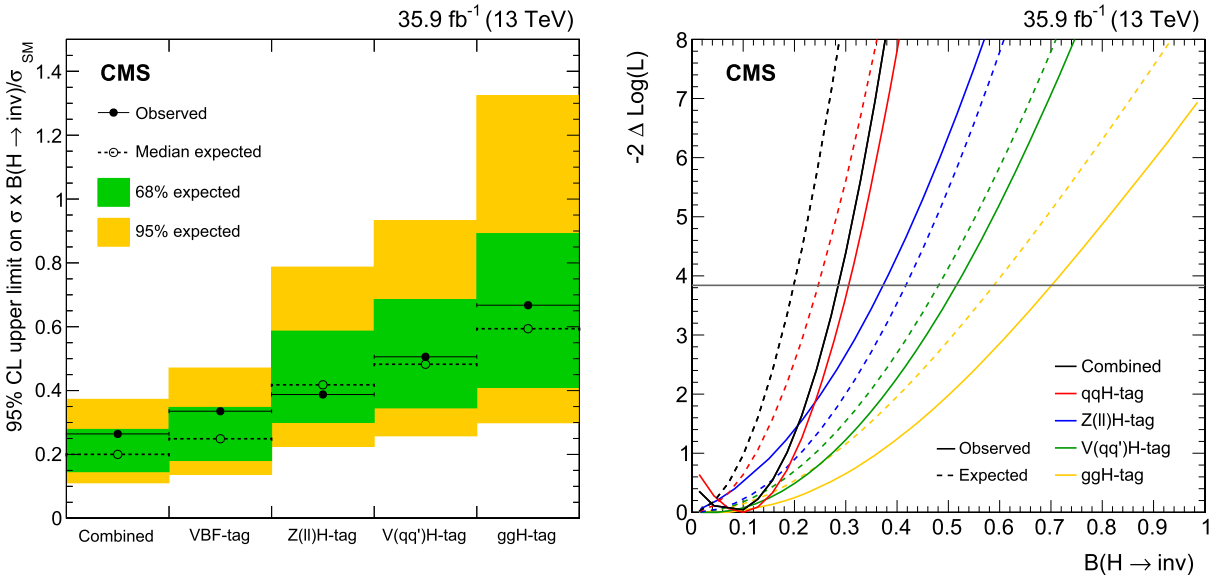

Fig. 8. On the left, observed and expected 95% CL upper limits on $(\sigma/\sigma_{SM})\,\mathcal{B}(H \to \text{inv})$ for both individual categories targeting VBF, Z($\ell\ell$)H, V(qq')H, and ggH production mode, as well as their combination, assuming an SM Higgs boson with a mass of 125.09 GeV. On the right, profile likelihood ratios as a function of $\mathcal{B}(H \to \text{inv})$. The solid curves represent the observations in data, while the dashed lines represent the expected result from a b-only fit. The observed and expected likelihood scans are reported for the full combination, as well as for the individual VBF, Z($\ell\ell$)H, V(qq′)H and ggH-tagged analyses.

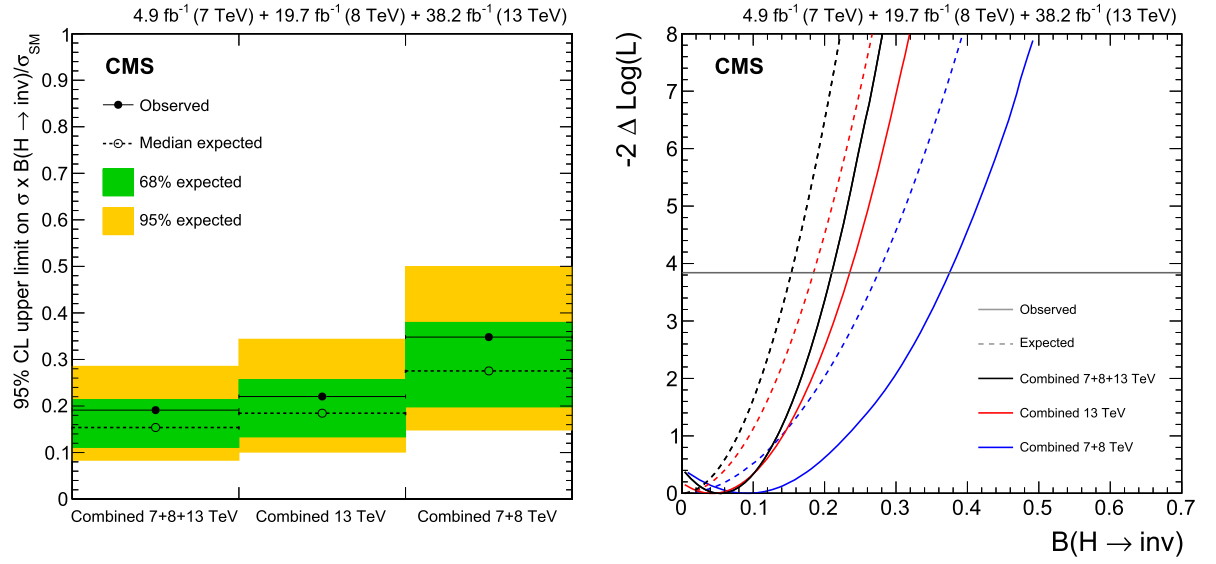

Fig. 9. On the left, observed and expected 95% CL upper limits on $(\sigma/\sigma_{SM})\,\mathcal{B}(H \to \text{inv})$ for partial combinations based either on 7+8 or 13 TeV data as well as their combination, assuming SM production cross sections for the Higgs boson with mass of 125.09 GeV. On the right, the corresponding profile likelihood ratios as a function of $\mathcal{B}(H \to \text{inv})$ are presented. The solid curves represent the observations in data, while the dashed lines represent the expected result obtained from the background-only hypothesis.

95% CL. The corresponding profile likelihood ratios as a function of $\mathcal{B}(H \to \text{inv})$ are shown in Fig. 9 (right). The measured value of the invisible branching fraction and an approximate 68% CL interval, obtained from the profile likelihood, are $\mathcal{B}(H \to \text{inv}) = 0.05 \pm 0.03\,(\text{stat}) \pm 0.07\,(\text{syst})$. The systematic uncertainties with the highest impact in the $\mathcal{B}(H \to \text{inv})$ measurement are the theoretical uncertainties affecting the Z($\nu\overline{\nu}$)/W($\ell\nu$) and ZZ/WW ratios in the VBF and Z($\ell\ell$)H channels, respectively, as well as the uncertainties in the lepton and photon reconstruction and identification efficiencies, jet energy scale, and veto efficiency of τ_h candidates.

The relative sensitivity of each search considered in the combination depends on the assumed SM production rates. The cross sections for the ggH, VBF and VH production modes are parametrized in terms of coupling strength modifiers κ_V and κ_F, which directly scale the coupling of the Higgs boson to vector bosons and fermions, respectively [69]. The contribution from the gg → ZH production is scaled to account for the interference between the tH and ZH diagrams, as described in Ref. [34]. In this context, SM production rates are obtained for $\kappa_V = \kappa_F = 1$. Fig. 10 (left) shows the observed 95% CL upper limits on $(\sigma/\sigma_{SM})\,\mathcal{B}(H \to \text{inv})$ evaluated as a function of κ_V and κ_F. The LHC best estimates for κ_V and κ_F from Ref. [4] are superimposed, along with the 68% and 95% CL limit contours. Within the 95% CL region, the observed (expected) upper limit on $\mathcal{B}(H \to \text{inv})$ varies between 0.14 (0.11) and 0.24 (0.19).

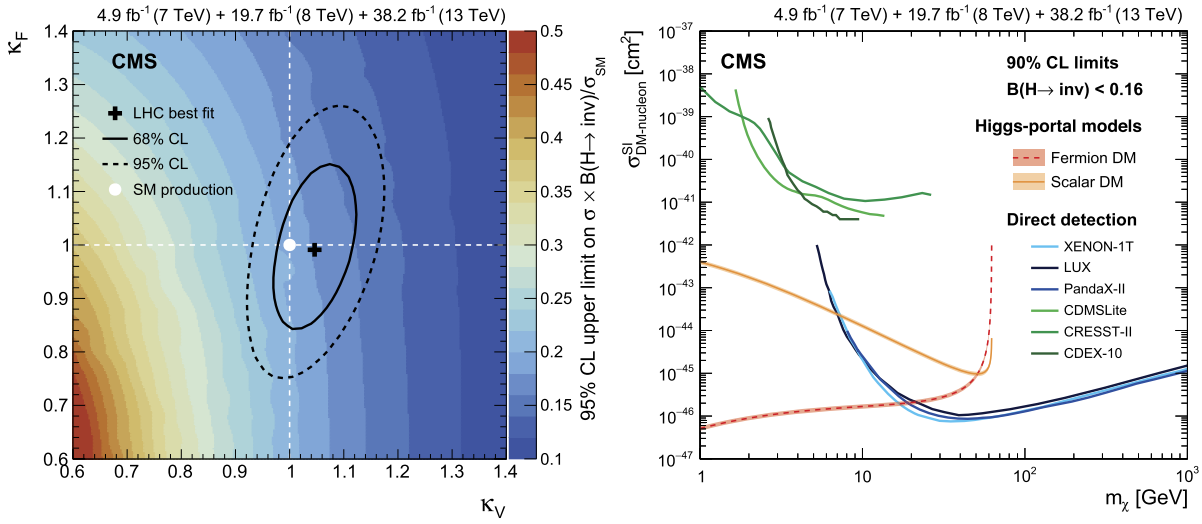

Fig. 10. On the left, observed 95% CL upper limits on $(\sigma/\sigma_{SM})\,\mathcal{B}(H \to \text{inv})$ for a Higgs boson with a mass of 125.09 GeV, whose production cross section varies as a function of the coupling modifiers κ_V and κ_F. Their best estimate, along with the 68% and 95% CL contours from Ref. [4], are also reported. The SM prediction corresponds to $\kappa_V = \kappa_F = 1$. On the right, 90% CL upper limits on the spin-independent DM-nucleon scattering cross section in Higgs-portal models, assuming a scalar (solid orange) or fermion (dashed red) DM candidate. Limits are computed as a function of m_χ and are compared to those from the XENON1T [79], LUX [80], PandaX-II [81], CDMSlite [82], CRESST-II [83], and CDEX-10 [84] experiments.

The upper limit on $\mathcal{B}(H \to \text{inv})$, obtained from the combination of $\sqrt{s} = 7$, 8, and 13 TeV searches, is interpreted in the context of Higgs-portal models of DM interactions, in which a stable DM particle couples to the SM Higgs boson. Direct-detection experiments are sensitive to the interaction between a DM particle and an atomic nucleus, which may be mediated by the exchange of a Higgs boson, producing nuclear recoil signatures that can be interpreted in terms of the DM-nucleon scattering cross section. The sensitivity of these experiments depends mainly on the DM particle mass (m_χ). If m_χ is smaller than half of the Higgs boson mass, the Higgs boson invisible width (Γ_{inv}) can be translated, within an effective field theory approach, into a spin-independent DM-nucleon elastic scattering cross section, as outlined in Ref. [9]. This translation is performed assuming that the DM candidate is either a scalar or a Majorana fermion, and both the central value and the uncertainty of the dimensionless nuclear form-factor f_N are taken from the recommendations of Ref. [78]. The conversion from $\mathcal{B}(H \to \text{inv})$ to Γ_{inv} uses the relation $\mathcal{B}(H \to \text{inv}) = \Gamma_{inv}/(\Gamma_{SM} + \Gamma_{inv})$, where Γ_{SM} is set to 4.07 MeV [69]. Since renormalizable models predicting a vectorial DM candidate require an extended dark Higgs sector, which may lead to modifications of kinematic distributions assumed for the invisible Higgs boson signal, such interpretation is not provided in the context of this Letter. Fig. 10 (right) shows the 90% CL upper limits on the spin-independent DM-nucleon scattering cross section as a function of m_χ, for both the scalar and the fermion DM scenarios. These limits are computed at 90% CL so that they can be compared with those from direct detection experiments such as XENON1T [79], LUX [80], PandaX-II [81], CDMSlite [82], CRESST-II [83], and CDEX-10 [84] which provide the strongest constraints in the m_χ range probed by this search. In the context of Higgs-portal models, the result presented in this Letter provides the most stringent limits for m_χ smaller than 18 (7) GeV, assuming a fermion (scalar) DM candidate.

10. Summary

A search for invisible decays of a Higgs boson is presented using proton-proton (pp) collision data at a center-of-mass energy $\sqrt{s} = 13$ TeV, collected by the CMS experiment in 2016 and corresponding to an integrated luminosity of 35.9 fb^{-1}. The search targets events in which a Higgs boson is produced through vector boson fusion (VBF). The data are found to be consistent with the predicted standard model (SM) backgrounds. An observed (expected) upper limit of 0.33 (0.25) is set, at 95% confidence level (CL), on the branching fraction of the Higgs boson decay to invisible particles, $\mathcal{B}(H \to \text{inv})$, by means of a binned likelihood fit to the dijet mass distribution. In addition, upper limits are set on the product of the cross section and branching fraction of an SM-like Higgs boson, with mass ranging between 110 and 1000 GeV.

A combination of CMS searches for the Higgs boson decaying to invisible particles, using pp collision data collected at $\sqrt{s} = 7$, 8, and 13 TeV (2015 and 2016), is also presented. The combination includes searches targeting Higgs boson production via VBF, in association with a vector boson (with hadronic decays of the W boson and hadronic or leptonic decays of the Z boson) and via gluon fusion with initial state radiation. The VBF search is the most sensitive channel involved in the combination. No significant deviations from the SM predictions are observed in any of these searches. The combination yields an observed (expected) upper limit on $\mathcal{B}(H \to \text{inv})$ of 0.19 (0.15) at 95% CL, assuming SM production rates for the Higgs boson and a Higgs boson mass of 125.09 GeV. The observed 90% CL upper limit of $\mathcal{B}(H \to \text{inv}) < 0.16$ is interpreted in terms of Higgs-portal models of dark matter (DM) interactions. Constraints are placed on the spin-independent DM-nucleon interaction cross section. When compared to the upper bounds from direct detection experiments, this limit provides the strongest constraints on fermion (scalar) DM particles with masses smaller than about 18 (7) GeV.

Acknowledgements

We congratulate our colleagues in the CERN accelerator departments for the excellent performance of the LHC and thank the technical and administrative staffs at CERN and at other CMS institutes for their contributions to the success of the CMS effort. In addition, we gratefully acknowledge the computing centres and personnel of the Worldwide LHC Computing Grid for delivering so effectively the computing infrastructure essential to our analyses. Finally, we acknowledge the enduring support for the construc-

tion and operation of the LHC and the CMS detector provided by the following funding agencies: BMWFW and FWF (Austria); FNRS and FWO (Belgium); CNPq, CAPES, FAPERJ, and FAPESP (Brazil); MES (Bulgaria); CERN; CAS, MOST, and NSFC (China); COLCIENCIAS (Colombia); MSES and CSF (Croatia); RPF (Cyprus); SENESCYT (Ecuador); MoER, ERC IUT, and ERDF (Estonia); Academy of Finland, MEC, and HIP (Finland); CEA and CNRS/IN2P3 (France); BMBF, DFG, and HGF (Germany); GSRT (Greece); NKFIA (Hungary); DAE and DST (India); IPM (Iran); SFI (Ireland); INFN (Italy); MSIP and NRF (Republic of Korea); LAS (Lithuania); MOE and UM (Malaysia); BUAP, CINVESTAV, CONACYT, LNS, SEP, and UASLP-FAI (Mexico); MBIE (New Zealand); PAEC (Pakistan); MSHE and NSC (Poland); FCT (Portugal); JINR (Dubna); MON, ROSATOM, RAS and RFBR (Russia); MESTD (Serbia); SEIDI, CPAN, PCTI and FEDER (Spain); Swiss Funding Agencies (Switzerland); MST (Taipei); ThEPCenter, IPST, STAR, and NSTDA (Thailand); TUBITAK and TAEK (Turkey); NASU and SFFR (Ukraine); STFC (United Kingdom); DOE and NSF (USA).

Individuals have received support from the Marie-Curie programme and the European Research Council and Horizon 2020 Grant, contract No. 675440 (European Union); the Leventis Foundation; the Alfred P. Sloan Foundation; the Alexander von Humboldt Foundation; the Belgian Federal Science Policy Office; the Fonds pour la Formation à la Recherche dans l'Industrie et dans l'Agriculture (FRIA-Belgium); the Agentschap voor Innovatie door Wetenschap en Technologie (IWT-Belgium); the F.R.S.-FNRS and FWO (Belgium) under the "Excellence of Science - EOS" - be.h project n. 30820817; the Ministry of Education, Youth and Sports (MEYS) of the Czech Republic; the Lendület ("Momentum") Programme and the János Bolyai Research Scholarship of the Hungarian Academy of Sciences, the New National Excellence Program ÚNKP, the NKFIA research grants 123842, 123959, 124845, 124850 and 125105 (Hungary); the Council of Science and Industrial Research, India; the HOMING PLUS programme of the Foundation for Polish Science, cofinanced from European Union, Regional Development Fund, the Mobility Plus programme of the Ministry of Science and Higher Education, the National Science Center (Poland), contracts Harmonia 2014/14/M/ST2/00428, Opus 2014/13/B/ST2/02543, 2014/15/B/ST2/03998, and 2015/19/B/ST2/02861, Sonata-bis 2012/07/E/ST2/01406; the National Priorities Research Program by Qatar National Research Fund; the Programa Estatal de Fomento de la Investigación Científica y Técnica de Excelencia María de Maeztu, grant MDM-2015-0509 and the Programa Severo Ochoa del Principado de Asturias; the Thalis and Aristeia programmes cofinanced by EU-ESF and the Greek NSRF; the Rachadapisek Sompot Fund for Postdoctoral Fellowship, Chulalongkorn University and the Chulalongkorn Academic into Its 2nd Century Project Advancement Project (Thailand); the Welch Foundation, contract C-1845; and the Weston Havens Foundation (USA).

References

[1] ATLAS Collaboration, Observation of a new particle in the search for the Standard Model Higgs boson with the ATLAS detector at the LHC, Phys. Lett. B 716 (2012) 1, https://doi.org/10.1016/j.physletb.2012.08.020, arXiv:1207.7214.

[2] CMS Collaboration, Observation of a new boson at a mass of 125 GeV with the CMS experiment at the LHC, Phys. Lett. B 716 (2012) 30, https://doi.org/10.1016/j.physletb.2012.08.021, arXiv:1207.7235.

[3] CMS Collaboration, Observation of a new boson with mass near 125 GeV in pp collisions at $\sqrt{s} = 7$ and 8 TeV, J. High Energy Phys. 06 (2013) 081, https://doi.org/10.1007/JHEP06(2013)081, arXiv:1303.4571.

[4] The ATLAS and CMS Collaborations, Measurements of the Higgs boson production and decay rates and constraints on its couplings from a combined ATLAS and CMS analysis of the LHC pp collision data at $\sqrt{s} = 7$ and 8 TeV, J. High Energy Phys. 08 (2016) 045, https://doi.org/10.1007/JHEP08(2016)045, arXiv:1606.02266.

[5] G. Bélanger, F. Boudjema, A. Cottrant, R.M. Godbole, A. Semenov, The MSSM invisible Higgs in the light of dark matter and g-2, Phys. Lett. B 519 (2001) 93, https://doi.org/10.1016/S0370-2693(01)00976-5, arXiv:hep-ph/0106275.

[6] A. Datta, K. Huitu, J. Laamanen, B. Mukhopadhyaya, Linear collider signals of an invisible Higgs boson in theories of large extra dimensions, Phys. Rev. D 70 (2004) 075003, https://doi.org/10.1103/PhysRevD.70.075003, arXiv:hep-ph/0404056.

[7] D. Dominici, J.F. Gunion, Invisible Higgs decays from Higgs-graviscalar mixing, Phys. Rev. D 80 (2009) 115006, https://doi.org/10.1103/PhysRevD.80.115006, arXiv:0902.1512.

[8] R.E. Shrock, M. Suzuki, Invisible decays of Higgs bosons, Phys. Lett. B 110 (1982) 250, https://doi.org/10.1016/0370-2693(82)91247-3.

[9] A. Djouadi, O. Lebedev, Y. Mambrini, J. Quevillon, Implications of LHC searches for Higgs–portal dark matter, Phys. Lett. B 709 (2012) 65, https://doi.org/10.1016/j.physletb.2012.01.062, arXiv:1112.3299.

[10] S. Baek, P. Ko, W.-I. Park, E. Senaha, Higgs portal vector dark matter: revisited, J. High Energy Phys. 05 (2013) 036, https://doi.org/10.1007/JHEP05(2013)036, arXiv:1212.2131.

[11] A. Djouadi, A. Falkowski, Y. Mambrini, J. Quevillon, Direct detection of Higgs–portal dark matter at the LHC, Eur. Phys. J. C 73 (2013) 2455, https://doi.org/10.1140/epjc/s10052-013-2455-1, arXiv:1205.3169.

[12] A. Beniwal, F. Rajec, C. Savage, P. Scott, C. Weniger, M. White, A.G. Williams, Combined analysis of effective Higgs–portal dark matter models, Phys. Rev. D 93 (2016) 115016, https://doi.org/10.1103/PhysRevD.93.115016, arXiv:1512.06458.

[13] ATLAS Collaboration, The ATLAS Experiment at the CERN Large Hadron Collider, J. Instrum. 3 (2008) S08003, https://doi.org/10.1088/1748-0221/3/08/S08003.

[14] ATLAS Collaboration, Constraints on new phenomena via Higgs boson couplings and invisible decays with the ATLAS detector, J. High Energy Phys. 11 (2015) 206, https://doi.org/10.1007/JHEP11(2015)206, arXiv:1509.00672.

[15] CMS Collaboration, The CMS experiment at the CERN LHC, J. Instrum. 3 (2008) S08004, https://doi.org/10.1088/1748-0221/3/08/S08004.

[16] CMS Collaboration, Searches for invisible decays of the Higgs boson in pp collisions at $\sqrt{s} = 7$, 8, and 13 TeV, J. High Energy Phys. 02 (2017) 135, https://doi.org/10.1007/JHEP02(2017)135, arXiv:1610.09218.

[17] O.J.P. Éboli, D. Zeppenfeld, Observing an invisible Higgs boson, Phys. Lett. B 495 (2000) 147, https://doi.org/10.1016/S0370-2693(00)01213-2, arXiv:hep-ph/0009158.

[18] CMS Collaboration, The CMS trigger system, J. Instrum. 12 (2017) P01020, https://doi.org/10.1088/1748-0221/12/01/P01020, arXiv:1609.02366.

[19] CMS Collaboration, Particle-flow reconstruction and global event description with the CMS detector, J. Instrum. 12 (2017) P10003, https://doi.org/10.1088/1748-0221/12/10/P10003, arXiv:1706.04965.

[20] M. Cacciari, G.P. Salam, G. Soyez, The anti-k_T jet clustering algorithm, J. High Energy Phys. 04 (2008) 063, https://doi.org/10.1088/1126-6708/2008/04/063, arXiv:0802.1189.

[21] M. Cacciari, G.P. Salam, G. Soyez, FastJet user manual, Eur. Phys. J. C 72 (2012) 1896, https://doi.org/10.1140/epjc/s10052-012-1896-2, arXiv:1111.6097.

[22] M. Cacciari, G.P. Salam, Pileup subtraction using jet areas, Phys. Lett. B 659 (2008) 119, https://doi.org/10.1016/j.physletb.2007.09.077, arXiv:0707.1378.

[23] CMS Collaboration, Jet energy scale and resolution in the CMS experiment in pp collisions at 8 TeV, J. Instrum. 12 (2017) P02014, https://doi.org/10.1088/1748-0221/12/02/P02014, arXiv:1607.03663.

[24] CMS Collaboration, Performance of the CMS missing transverse momentum reconstruction in pp data at $\sqrt{s} = 8$ TeV, J. Instrum. 10 (2015) P02006, https://doi.org/10.1088/1748-0221/10/02/P02006, arXiv:1411.0511.

[25] CMS Collaboration, Performance of CMS muon reconstruction in pp collision events at $\sqrt{s} = 7$ TeV, J. Instrum. 7 (2012) P10002, https://doi.org/10.1088/1748-0221/7/10/P10002, arXiv:1206.4071.

[26] CMS Collaboration, Performance of electron reconstruction and selection with the CMS detector in proton-proton collisions at $\sqrt{s} = 8$ TeV, J. Instrum. 10 (2015) P06005, https://doi.org/10.1088/1748-0221/10/06/P06005, arXiv:1502.02701.

[27] CMS Collaboration, Performance of photon reconstruction and identification with the CMS detector in proton-proton collisions at $\sqrt{s} = 8$ TeV, J. Instrum. 10 (2015) P08010, https://doi.org/10.1088/1748-0221/10/08/P08010, arXiv:1502.02702.

[28] CMS Collaboration, Reconstruction and identification of τ lepton decays to hadrons and ν_τ at CMS, J. Instrum. 11 (2016) P01019, https://doi.org/10.1088/1748-0221/11/01/P01019, arXiv:1510.07488.

[29] P. Nason, A new method for combining NLO QCD with shower Monte Carlo algorithms, J. High Energy Phys. 11 (2004) 040, https://doi.org/10.1088/1126-6708/2004/11/040, arXiv:hep-ph/0409146.

[30] S. Frixione, P. Nason, C. Oleari, Matching NLO QCD computations with parton shower simulations: the POWHEG method, J. High Energy Phys. 11 (2007) 070, https://doi.org/10.1088/1126-6708/2007/11/070, arXiv:0709.2092.

[31] S. Alioli, P. Nason, C. Oleari, E. Re, A general framework for implementing NLO calculations in shower Monte Carlo programs: the POWHEG BOX, J. High Energy Phys. 06 (2010) 043, https://doi.org/10.1007/JHEP06(2010)043, arXiv:1002.2581.

[32] E. Bagnaschi, G. Degrassi, P. Slavich, A. Vicini, Higgs production via gluon fusion in the POWHEG approach in the SM and in the MSSM, J. High Energy Phys. 02 (2012) 088, https://doi.org/10.1007/JHEP02(2012)088, arXiv:1111.2854.

[33] P. Nason, C. Oleari, NLO Higgs boson production via vector-boson fusion matched with shower in POWHEG, J. High Energy Phys. 02 (2010) 037, https://doi.org/10.1007/JHEP02(2010)037, arXiv:0911.5299.

[34] LHC Higgs Cross Section Working Group, Handbook of LHC Higgs cross sections: 4. Deciphering the nature of the Higgs sector, https://doi.org/10.23731/CYRM-2017-002, arXiv:1610.07922, 2016.

[35] C. Anastasiou, C. Duhr, F. Dulat, E. Furlan, T. Gehrmann, F. Herzog, A. Lazopoulos, B. Mistlberger, High precision determination of the gluon fusion Higgs boson cross-section at the LHC, J. High Energy Phys. 05 (2016) 058, https://doi.org/10.1007/JHEP05(2016)058, arXiv:1602.00695.

[36] D. de Florian, G. Ferrera, M. Grazzini, D. Tommasini, Higgs boson production at the LHC: transverse momentum resummation effects in the $H \to \gamma\gamma$, $H \to WW \to \ell\nu\ell\nu$ and $H \to ZZ \to 4\ell$ decay modes, J. High Energy Phys. 06 (2012) 132, https://doi.org/10.1007/JHEP06(2012)132, arXiv:1203.6321.

[37] M. Grazzini, H. Sargsyan, Heavy-quark mass effects in Higgs boson production at the LHC, J. High Energy Phys. 09 (2013) 129, https://doi.org/10.1007/JHEP09(2013)129, arXiv:1306.4581.

[38] The ATLAS and CMS Collaborations, Combined measurement of the Higgs boson mass in pp collisions at $\sqrt{s} = 7$ and 8 TeV with the ATLAS and CMS experiments, Phys. Rev. Lett. 114 (2015) 191803, https://doi.org/10.1103/PhysRevLett.114.191803, arXiv:1503.07589.

[39] CMS Collaboration, Measurements of properties of the Higgs boson decaying into the four-lepton final state in pp collisions at $\sqrt{s} = 13$ TeV, J. High Energy Phys. 11 (2017) 047, https://doi.org/10.1007/JHEP11(2017)047, arXiv:1706.09936.

[40] J. Alwall, R. Frederix, S. Frixione, V. Hirschi, F. Maltoni, O. Mattelaer, H.S. Shao, T. Stelzer, P. Torrielli, M. Zaro, The automated computation of tree-level and next-to-leading order differential cross sections, and their matching to parton shower simulations, J. High Energy Phys. 07 (2014) 079, https://doi.org/10.1007/JHEP07(2014)079, arXiv:1405.0301.

[41] J.M. Campbell, R.K. Ellis, P. Nason, E. Re, Top-pair production and decay at NLO matched with parton showers, J. High Energy Phys. 04 (2015) 114, https://doi.org/10.1007/JHEP04(2015)114, arXiv:1412.1828.

[42] S. Alioli, P. Nason, C. Oleari, E. Re, NLO single-top production matched with shower in POWHEG: s- and t-channel contributions, J. High Energy Phys. 09 (2009) 111, https://doi.org/10.1007/JHEP02(2010)011, arXiv:0907.4076, Erratum: J. High Energy Phys. 02 (2010) 011.

[43] E. Re, Single-top Wt-channel production matched with parton showers using the POWHEG method, Eur. Phys. J. C 71 (2011) 1547, https://doi.org/10.1140/epjc/s10052-011-1547-z, arXiv:1009.2450.

[44] T. Sjöstrand, S. Ask, J.R. Christiansen, R. Corke, N. Desai, P. Ilten, S. Mrenna, S. Prestel, C.O. Rasmussen, P.Z. Skands, An introduction to PYTHIA 8.2, Comput. Phys. Commun. 191 (2015) 159, https://doi.org/10.1016/j.cpc.2015.01.024, arXiv:1410.3012.

[45] T. Melia, P. Nason, R. Rontsch, G. Zanderighi, W^+W^-, WZ and ZZ production in the POWHEG BOX, J. High Energy Phys. 11 (2011) 078, https://doi.org/10.1007/JHEP11(2011)078, arXiv:1107.5051.

[46] CMS Collaboration, Event generator tunes obtained from underlying event and multiparton scattering measurements, Eur. Phys. J. C 76 (2016) 155, https://doi.org/10.1140/epjc/s10052-016-3988-x, arXiv:1512.00815.

[47] J. Alwall, et al., Comparative study of various algorithms for the merging of parton showers and matrix elements in hadronic collisions, Eur. Phys. J. C 53 (2008) 473, https://doi.org/10.1140/epjc/s10052-007-0490-5, arXiv:0706.2569.

[48] R. Frederix, S. Frixione, Merging meets matching in MC@NLO, J. High Energy Phys. 12 (2012) 061, https://doi.org/10.1007/JHEP12(2012)061, arXiv:1209.6215.

[49] R.D. Ball, et al., NNPDF, Parton distributions for the LHC Run II, J. High Energy Phys. 04 (2015) 040, https://doi.org/10.1007/JHEP04(2015)040, arXiv:1410.8849.

[50] S. Agostinelli, et al., GEANT4, GEANT4 — a simulation toolkit, Nucl. Instrum. Methods Phys. Res., Sect. A 506 (2003) 250, https://doi.org/10.1016/S0168-9002(03)01368-8.

[51] CMS Collaboration, Performance of Missing Energy Reconstruction in 13 TeV pp Collision Data Using the CMS Detector, CMS Physics Analysis Summary CMS-PAS-JME-16-004, 2016, https://cds.cern.ch/record/2205284.

[52] CMS Collaboration, Identification of heavy-flavour jets with the CMS detector in pp collisions at 13 TeV, J. Instrum. 13 (2018) P05011, https://doi.org/10.1088/1748-0221/13/05/P05011, arXiv:1712.07158.

[53] J.M. Lindert, et al., Precise predictions for V+jets dark matter backgrounds, Eur. Phys. J. C 77 (2017) 829, https://doi.org/10.1140/epjc/s10052-017-5389-1, arXiv:1705.04664.

[54] K. Arnold, et al., VBFNLO: a parton level Monte Carlo for processes with electroweak bosons, Comput. Phys. Commun. 180 (2009) 1661, https://doi.org/10.1016/j.cpc.2009.03.006, arXiv:0811.4559.

[55] J. Baglio, J. Bellm, F. Campanario, B. Feigl, J. Frank, T. Figy, M. Kerner, L.D. Ninh, S. Palmer, M. Rauch, R. Roth, F. Schissler, O. Schlimpert, D. Zeppenfeld, Release note — VBFNLO 2.7.0, arXiv:1404.3940, 2014.

[56] CMS Collaboration, Search for new physics with jets and missing transverse momentum in pp collisions at $\sqrt{s} = 7$ TeV, J. High Energy Phys. 08 (2011) 155, https://doi.org/10.1007/JHEP08(2011)155, arXiv:1106.4503.

[57] M. Czakon, D. Heymes, A. Mitov, High-precision differential predictions for top-quark pairs at the LHC, Phys. Rev. Lett. 116 (2016) 082003, https://doi.org/10.1103/PhysRevLett.116.082003, arXiv:1511.00549.

[58] CMS Collaboration, Measurement of the ZZ production cross section and $Z \to \ell^+\ell^-\ell'^+\ell'^-$ branching fraction in pp collisions at $\sqrt{s} = 13$ TeV, Phys. Lett. B 763 (2016) 280, https://doi.org/10.1016/j.physletb.2016.10.054, arXiv:1607.08834.

[59] CMS Collaboration, Measurement of the WZ production cross section in pp collisions at $\sqrt{s} = 13$ TeV, Phys. Lett. B 766 (2017) 268, https://doi.org/10.1016/j.physletb.2017.01.011, arXiv:1607.06943.

[60] CMS Collaboration, CMS Luminosity Measurements for the 2016 Data Taking Period, CMS Physics Analysis Summary, CMS-PAS-LUM-17-001, 2017, https://cds.cern.ch/record/2257069.

[61] S. Baker, R.D. Cousins, Clarification of the use of chi-square and likelihood functions in fits to histograms, Nucl. Instrum. Methods 221 (1984) 437, https://doi.org/10.1016/0167-5087(84)90016-4.

[62] J.K. Lindsey, Parametric Statistical Inference, Oxford Science Publications, Clarendon Press, 1996.

[63] T. Junk, Confidence level computation for combining searches with small statistics, Nucl. Instrum. Methods Phys. Res., Sect. A 434 (1999) 435, https://doi.org/10.1016/S0168-9002(99)00498-2, arXiv:hep-ex/9902006.

[64] A.L. Read, Presentation of search results: the CL_s technique, J. Phys. G 28 (2002) 2693, https://doi.org/10.1088/0954-3899/28/10/313.

[65] G. Cowan, K. Cranmer, E. Gross, O. Vitells, Asymptotic formulae for likelihood-based tests of new physics, Eur. Phys. J. C 71 (2011) 1554, https://doi.org/10.1140/epjc/s10052-011-1554-0, arXiv:1007.1727, Erratum: https://doi.org/10.1140/epjc/s10052-013-2501-z.

[66] The ATLAS and CMS Collaborations, the LHC Higgs Combination Group, Procedure for the LHC Higgs Boson Search Combination in Summer 2011, Technical Report CMS-NOTE-2011-005, ATL-PHYS-PUB-2011-11, 2011, https://cds.cern.ch/record/1379837.

[67] K. Hamilton, P. Nason, G. Zanderighi, MINLO: multi-scale improved NLO, J. High Energy Phys. 10 (2012) 155, https://doi.org/10.1007/JHEP10(2012)155, arXiv:1206.3572.

[68] CMS Collaboration, Simplified Likelihood for the Re-Interpretation of Public CMS Results, Technical Report, CMS-NOTE-2017-001, 2017, https://cds.cern.ch/record/2242860.

[69] LHC Higgs Cross Section Working Group, Handbook of LHC Higgs cross sections: 3. Higgs properties, https://doi.org/10.5170/CERN-2013-004, arXiv:1307.1347, 2013.

[70] CMS Collaboration, Search for invisible decays of Higgs bosons in the vector boson fusion and associated ZH production modes, Eur. Phys. J. C 74 (2014) 2980, https://doi.org/10.1140/epjc/s10052-014-2980-6, arXiv:1404.1344.

[71] CMS Collaboration, Search for a Higgs boson in the mass range from 145 to 1000 GeV decaying to a pair of W or Z bosons, J. High Energy Phys. 10 (2015) 144, https://doi.org/10.1007/JHEP10(2015)144, arXiv:1504.00936.

[72] CMS Collaboration, Search for new physics in events with a leptonically decaying Z boson and a large transverse momentum imbalance in proton-proton collisions at $\sqrt{s} = 13$ TeV, Eur. Phys. J. C 78 (2018) 291, https://doi.org/10.1140/epjc/s10052-018-5740-1, arXiv:1711.00431.

[73] CMS Collaboration, Search for new physics in final states with an energetic jet or a hadronically decaying W or Z boson and transverse momentum imbalance at $\sqrt{s} = 13$ TeV, Phys. Rev. D 97 (2018) 092005, https://doi.org/10.1103/PhysRevD.97.092005, arXiv:1712.02345.

[74] CMS Collaboration, Search for dark matter in proton-proton collisions at 8 TeV with missing transverse momentum and vector boson tagged jets, J. High Energy Phys. 12 (2016) 083, https://doi.org/10.1007/JHEP12(2016)083, arXiv:1607.05764.

[75] CMS Collaboration, Absolute Calibration of the Luminosity Measurement at CMS: Winter 2012 Update, CMS Physics Analysis Summary, CMS-PAS-SMP-12-008, 2012, https://cds.cern.ch/record/1598864.

[76] CMS Collaboration, CMS Luminosity Based on Pixel Cluster Counting - Summer 2013 Update, CMS Physics Analysis Summary, CMS-PAS-LUM-13-001, 2013, https://cds.cern.ch/record/1598864.

[77] CMS Collaboration, CMS Luminosity Measurements for the 2015 Data Taking Period, CMS Physics Analysis Summary, CMS-PAS-LUM-15-001, 2017, https://cds.cern.ch/record/2138682.

[78] M. Hoferichter, P. Klos, J. Menéndez, A. Schwenk, Improved limits for Higgs-portal dark matter from LHC searches, Phys. Rev. Lett. 119 (2017) 181803, https://doi.org/10.1103/PhysRevLett.119.181803, arXiv:1708.02245.

[79] E. Aprile, et al., XENON, Dark matter search results from a one ton-year exposure of XENON1T, Phys. Rev. Lett. 121 (2018) 111302, https://doi.org/10.1103/PhysRevLett.121.111302, arXiv:1805.12562.

[80] D.S. Akerib, et al., LUX, Results from a search for dark matter in the complete LUX exposure, Phys. Rev. Lett. 118 (2017) 021303, https://doi.org/10.1103/PhysRevLett.118.021303, arXiv:1608.07648.

[81] A. Tan, et al., PandaX-II, Dark matter results from first 98.7 days of data from the PandaX-II experiment, Phys. Rev. Lett. 117 (2016) 121303, https://doi.org/10.1103/PhysRevLett.117.121303, arXiv:1607.07400.
[82] R. Agnese, et al., SuperCDMS, New results from the search for low-mass weakly interacting massive particles with the CDMS low ionization threshold experiment, Phys. Rev. Lett. 116 (2016) 071301, https://doi.org/10.1103/PhysRevLett.116.071301, arXiv:1509.02448.
[83] G. Angloher, et al., CRESST, Results on light dark matter particles with a low-threshold CRESST-II detector, Eur. Phys. J. C 76 (2016) 25, https://doi.org/10.1140/epjc/s10052-016-3877-3, arXiv:1509.01515.
[84] H. Jiang, et al., CDEX, Limits on light weakly interacting massive particles from the first 102.8 kg × day data of the CDEX-10 experiment, Phys. Rev. Lett. 120 (2018) 241301, https://doi.org/10.1103/PhysRevLett.120.241301, arXiv:1802.09016.

The CMS Collaboration

A.M. Sirunyan, A. Tumasyan

Yerevan Physics Institute, Yerevan, Armenia

W. Adam, F. Ambrogi, E. Asilar, T. Bergauer, J. Brandstetter, M. Dragicevic, J. Erö, A. Escalante Del Valle, M. Flechl, R. Frühwirth [1], V.M. Ghete, J. Hrubec, M. Jeitler [1], N. Krammer, I. Krätschmer, D. Liko, T. Madlener, I. Mikulec, N. Rad, H. Rohringer, J. Schieck [1], R. Schöfbeck, M. Spanring, D. Spitzbart, A. Taurok, W. Waltenberger, J. Wittmann, C.-E. Wulz [1], M. Zarucki

Institut für Hochenergiephysik, Wien, Austria

V. Chekhovsky, V. Mossolov, J. Suarez Gonzalez

Institute for Nuclear Problems, Minsk, Belarus

E.A. De Wolf, D. Di Croce, X. Janssen, J. Lauwers, M. Pieters, M. Van De Klundert, H. Van Haevermaet, P. Van Mechelen, N. Van Remortel

Universiteit Antwerpen, Antwerpen, Belgium

S. Abu Zeid, F. Blekman, J. D'Hondt, I. De Bruyn, J. De Clercq, K. Deroover, G. Flouris, D. Lontkovskyi, S. Lowette, I. Marchesini, S. Moortgat, L. Moreels, Q. Python, K. Skovpen, S. Tavernier, W. Van Doninck, P. Van Mulders, I. Van Parijs

Vrije Universiteit Brussel, Brussel, Belgium

D. Beghin, B. Bilin, H. Brun, B. Clerbaux, G. De Lentdecker, H. Delannoy, B. Dorney, G. Fasanella, L. Favart, R. Goldouzian, A. Grebenyuk, A.K. Kalsi, T. Lenzi, J. Luetic, N. Postiau, E. Starling, L. Thomas, C. Vander Velde, P. Vanlaer, D. Vannerom, Q. Wang

Université Libre de Bruxelles, Bruxelles, Belgium

T. Cornelis, D. Dobur, A. Fagot, M. Gul, I. Khvastunov [2], D. Poyraz, C. Roskas, D. Trocino, M. Tytgat, W. Verbeke, B. Vermassen, M. Vit, N. Zaganidis

Ghent University, Ghent, Belgium

H. Bakhshiansohi, O. Bondu, S. Brochet, G. Bruno, C. Caputo, P. David, C. Delaere, M. Delcourt, B. Francois, A. Giammanco, G. Krintiras, V. Lemaitre, A. Magitteri, A. Mertens, M. Musich, K. Piotrzkowski, A. Saggio, M. Vidal Marono, S. Wertz, J. Zobec

Université Catholique de Louvain, Louvain-la-Neuve, Belgium

F.L. Alves, G.A. Alves, L. Brito, M. Correa Martins Junior, G. Correia Silva, C. Hensel, A. Moraes, M.E. Pol, P. Rebello Teles

Centro Brasileiro de Pesquisas Fisicas, Rio de Janeiro, Brazil

E. Belchior Batista Das Chagas, W. Carvalho, J. Chinellato [3], E. Coelho, E.M. Da Costa, G.G. Da Silveira [4], D. De Jesus Damiao, C. De Oliveira Martins, S. Fonseca De Souza, H. Malbouisson, D. Matos Figueiredo,

M. Melo De Almeida, C. Mora Herrera, L. Mundim, H. Nogima, W.L. Prado Da Silva, L.J. Sanchez Rosas, A. Santoro, A. Sznajder, M. Thiel, E.J. Tonelli Manganote [3], F. Torres Da Silva De Araujo, A. Vilela Pereira

Universidade do Estado do Rio de Janeiro, Rio de Janeiro, Brazil

S. Ahuja [a], C.A. Bernardes [a], L. Calligaris [a], T.R. Fernandez Perez Tomei [a], E.M. Gregores [b], P.G. Mercadante [b], S.F. Novaes [a], S.S. Padula [a], D. Romero Abad [b]

[a] *Universidade Estadual Paulista, São Paulo, Brazil*
[b] *Universidade Federal do ABC, São Paulo, Brazil*

A. Aleksandrov, R. Hadjiiska, P. Iaydjiev, A. Marinov, M. Misheva, M. Rodozov, M. Shopova, G. Sultanov

Institute for Nuclear Research and Nuclear Energy, Bulgarian Academy of Sciences, Sofia, Bulgaria

A. Dimitrov, L. Litov, B. Pavlov, P. Petkov

University of Sofia, Sofia, Bulgaria

W. Fang [5], X. Gao [5], L. Yuan

Beihang University, Beijing, China

M. Ahmad, J.G. Bian, G.M. Chen, H.S. Chen, M. Chen, Y. Chen, C.H. Jiang, D. Leggat, H. Liao, Z. Liu, F. Romeo, S.M. Shaheen [6], A. Spiezia, J. Tao, C. Wang, Z. Wang, E. Yazgan, H. Zhang, J. Zhao

Institute of High Energy Physics, Beijing, China

Y. Ban, G. Chen, A. Levin, J. Li, L. Li, Q. Li, Y. Mao, S.J. Qian, D. Wang, Z. Xu

State Key Laboratory of Nuclear Physics and Technology, Peking University, Beijing, China

Y. Wang

Tsinghua University, Beijing, China

C. Avila, A. Cabrera, C.A. Carrillo Montoya, L.F. Chaparro Sierra, C. Florez, C.F. González Hernández, M.A. Segura Delgado

Universidad de Los Andes, Bogota, Colombia

B. Courbon, N. Godinovic, D. Lelas, I. Puljak, T. Sculac

University of Split, Faculty of Electrical Engineering, Mechanical Engineering and Naval Architecture, Split, Croatia

Z. Antunovic, M. Kovac

University of Split, Faculty of Science, Split, Croatia

V. Brigljevic, D. Ferencek, K. Kadija, B. Mesic, A. Starodumov [7], T. Susa

Institute Rudjer Boskovic, Zagreb, Croatia

M.W. Ather, A. Attikis, M. Kolosova, G. Mavromanolakis, J. Mousa, C. Nicolaou, F. Ptochos, P.A. Razis, H. Rykaczewski

University of Cyprus, Nicosia, Cyprus

M. Finger [8], M. Finger Jr. [8]

Charles University, Prague, Czech Republic

E. Ayala

Escuela Politecnica Nacional, Quito, Ecuador

E. Carrera Jarrin

Universidad San Francisco de Quito, Quito, Ecuador

H. Abdalla [9], A.A. Abdelalim [10,11], A. Mohamed [11]

Academy of Scientific Research and Technology of the Arab Republic of Egypt, Egyptian Network of High Energy Physics, Cairo, Egypt

S. Bhowmik, A. Carvalho Antunes De Oliveira, R.K. Dewanjee, K. Ehataht, M. Kadastik, M. Raidal, C. Veelken

National Institute of Chemical Physics and Biophysics, Tallinn, Estonia

P. Eerola, H. Kirschenmann, J. Pekkanen, M. Voutilainen

Department of Physics, University of Helsinki, Helsinki, Finland

J. Havukainen, J.K. Heikkilä, T. Järvinen, V. Karimäki, R. Kinnunen, T. Lampén, K. Lassila-Perini, S. Laurila, S. Lehti, T. Lindén, P. Luukka, T. Mäenpää, H. Siikonen, E. Tuominen, J. Tuominiemi

Helsinki Institute of Physics, Helsinki, Finland

T. Tuuva

Lappeenranta University of Technology, Lappeenranta, Finland

M. Besancon, F. Couderc, M. Dejardin, D. Denegri, J.L. Faure, F. Ferri, S. Ganjour, A. Givernaud, P. Gras, G. Hamel de Monchenault, P. Jarry, C. Leloup, E. Locci, J. Malcles, G. Negro, J. Rander, A. Rosowsky, M.Ö. Sahin, M. Titov

IRFU, CEA, Université Paris-Saclay, Gif-sur-Yvette, France

A. Abdulsalam [12], C. Amendola, I. Antropov, F. Beaudette, P. Busson, C. Charlot, R. Granier de Cassagnac, I. Kucher, S. Lisniak, A. Lobanov, J. Martin Blanco, M. Nguyen, C. Ochando, G. Ortona, P. Paganini, P. Pigard, R. Salerno, J.B. Sauvan, Y. Sirois, A.G. Stahl Leiton, A. Zabi, A. Zghiche

Laboratoire Leprince-Ringuet, Ecole polytechnique, CNRS/IN2P3, Université Paris-Saclay, Palaiseau, France

J.-L. Agram [13], J. Andrea, D. Bloch, J.-M. Brom, E.C. Chabert, V. Cherepanov, C. Collard, E. Conte [13], J.-C. Fontaine [13], D. Gelé, U. Goerlach, M. Jansová, A.-C. Le Bihan, N. Tonon, P. Van Hove

Université de Strasbourg, CNRS, IPHC UMR 7178, Strasbourg, France

S. Gadrat

Centre de Calcul de l'Institut National de Physique Nucleaire et de Physique des Particules, CNRS/IN2P3, Villeurbanne, France

S. Beauceron, C. Bernet, G. Boudoul, N. Chanon, R. Chierici, D. Contardo, P. Depasse, H. El Mamouni, J. Fay, L. Finco, S. Gascon, M. Gouzevitch, G. Grenier, B. Ille, F. Lagarde, I.B. Laktineh, H. Lattaud, M. Lethuillier, L. Mirabito, A.L. Pequegnot, S. Perries, A. Popov [14], V. Sordini, M. Vander Donckt, S. Viret, S. Zhang

Université de Lyon, Université Claude Bernard Lyon 1, CNRS-IN2P3, Institut de Physique Nucléaire de Lyon, Villeurbanne, France

A. Khvedelidze [8]

Georgian Technical University, Tbilisi, Georgia

Z. Tsamalaidze [8]

Tbilisi State University, Tbilisi, Georgia

C. Autermann, L. Feld, M.K. Kiesel, K. Klein, M. Lipinski, M. Preuten, M.P. Rauch, C. Schomakers, J. Schulz, M. Teroerde, B. Wittmer, V. Zhukov [14]

RWTH Aachen University, I. Physikalisches Institut, Aachen, Germany

A. Albert, D. Duchardt, M. Endres, M. Erdmann, T. Esch, R. Fischer, S. Ghosh, A. Güth, T. Hebbeker, C. Heidemann, K. Hoepfner, H. Keller, S. Knutzen, L. Mastrolorenzo, M. Merschmeyer, A. Meyer, P. Millet, S. Mukherjee, T. Pook, M. Radziej, H. Reithler, M. Rieger, F. Scheuch, A. Schmidt, D. Teyssier

RWTH Aachen University, III. Physikalisches Institut A, Aachen, Germany

G. Flügge, O. Hlushchenko, B. Kargoll, T. Kress, A. Künsken, T. Müller, A. Nehrkorn, A. Nowack, C. Pistone, O. Pooth, H. Sert, A. Stahl [15]

RWTH Aachen University, III. Physikalisches Institut B, Aachen, Germany

M. Aldaya Martin, T. Arndt, C. Asawatangtrakuldee, I. Babounikau, K. Beernaert, O. Behnke, U. Behrens, A. Bermúdez Martínez, D. Bertsche, A.A. Bin Anuar, K. Borras [16], V. Botta, A. Campbell, P. Connor, C. Contreras-Campana, F. Costanza, V. Danilov, A. De Wit, M.M. Defranchis, C. Diez Pardos, D. Domínguez Damiani, G. Eckerlin, T. Eichhorn, A. Elwood, E. Eren, E. Gallo [17], A. Geiser, J.M. Grados Luyando, A. Grohsjean, P. Gunnellini, M. Guthoff, M. Haranko, A. Harb, J. Hauk, H. Jung, M. Kasemann, J. Keaveney, C. Kleinwort, J. Knolle, D. Krücker, W. Lange, A. Lelek, T. Lenz, K. Lipka, W. Lohmann [18], R. Mankel, I.-A. Melzer-Pellmann, A.B. Meyer, M. Meyer, M. Missiroli, G. Mittag, J. Mnich, V. Myronenko, S.K. Pflitsch, D. Pitzl, A. Raspereza, M. Savitskyi, P. Saxena, P. Schütze, C. Schwanenberger, R. Shevchenko, A. Singh, N. Stefaniuk, H. Tholen, O. Turkot, A. Vagnerini, G.P. Van Onsem, R. Walsh, Y. Wen, K. Wichmann, C. Wissing, O. Zenaiev

Deutsches Elektronen-Synchrotron, Hamburg, Germany

R. Aggleton, S. Bein, L. Benato, A. Benecke, V. Blobel, M. Centis Vignali, T. Dreyer, E. Garutti, D. Gonzalez, J. Haller, A. Hinzmann, A. Karavdina, G. Kasieczka, R. Klanner, R. Kogler, N. Kovalchuk, S. Kurz, V. Kutzner, J. Lange, D. Marconi, J. Multhaup, M. Niedziela, D. Nowatschin, A. Perieanu, A. Reimers, O. Rieger, C. Scharf, P. Schleper, S. Schumann, J. Schwandt, J. Sonneveld, H. Stadie, G. Steinbrück, F.M. Stober, M. Stöver, D. Troendle, A. Vanhoefer, B. Vormwald

University of Hamburg, Hamburg, Germany

M. Akbiyik, C. Barth, M. Baselga, S. Baur, E. Butz, R. Caspart, T. Chwalek, F. Colombo, W. De Boer, A. Dierlamm, N. Faltermann, B. Freund, M. Giffels, M.A. Harrendorf, F. Hartmann [15], S.M. Heindl, U. Husemann, F. Kassel [15], I. Katkov [14], S. Kudella, H. Mildner, S. Mitra, M.U. Mozer, Th. Müller, M. Plagge, G. Quast, K. Rabbertz, M. Schröder, I. Shvetsov, G. Sieber, H.J. Simonis, R. Ulrich, S. Wayand, M. Weber, T. Weiler, S. Williamson, C. Wöhrmann, R. Wolf

Karlsruher Institut fuer Technologie, Karlsruhe, Germany

G. Anagnostou, G. Daskalakis, T. Geralis, A. Kyriakis, D. Loukas, G. Paspalaki, I. Topsis-Giotis

Institute of Nuclear and Particle Physics (INPP), NCSR Demokritos, Aghia Paraskevi, Greece

G. Karathanasis, S. Kesisoglou, P. Kontaxakis, A. Panagiotou, N. Saoulidou, E. Tziaferi, K. Vellidis

National and Kapodistrian University of Athens, Athens, Greece

K. Kousouris, I. Papakrivopoulos, G. Tsipolitis

National Technical University of Athens, Athens, Greece

I. Evangelou, C. Foudas, P. Gianneios, P. Katsoulis, P. Kokkas, S. Mallios, N. Manthos, I. Papadopoulos, E. Paradas, J. Strologas, F.A. Triantis, D. Tsitsonis

University of Ioánnina, Ioánnina, Greece

M. Bartók [19], M. Csanad, N. Filipovic, P. Major, M.I. Nagy, G. Pasztor, O. Surányi, G.I. Veres

MTA-ELTE Lendület CMS Particle and Nuclear Physics Group, Eötvös Loránd University, Budapest, Hungary

G. Bencze, C. Hajdu, D. Horvath [20], Á. Hunyadi, F. Sikler, T.Á. Vámi, V. Veszpremi, G. Vesztergombi [†]

Wigner Research Centre for Physics, Budapest, Hungary

N. Beni, S. Czellar, J. Karancsi [21], A. Makovec, J. Molnar, Z. Szillasi

Institute of Nuclear Research ATOMKI, Debrecen, Hungary

P. Raics, Z.L. Trocsanyi, B. Ujvari

Institute of Physics, University of Debrecen, Debrecen, Hungary

S. Choudhury, J.R. Komaragiri, P.C. Tiwari

Indian Institute of Science (IISc), Bangalore, India

S. Bahinipati [22], C. Kar, P. Mal, K. Mandal, A. Nayak [23], D.K. Sahoo [22], S.K. Swain

National Institute of Science Education and Research, HBNI, Bhubaneswar, India

S. Bansal, S.B. Beri, V. Bhatnagar, S. Chauhan, R. Chawla, N. Dhingra, R. Gupta, A. Kaur, A. Kaur, M. Kaur, S. Kaur, R. Kumar, P. Kumari, M. Lohan, A. Mehta, K. Sandeep, S. Sharma, J.B. Singh, G. Walia

Panjab University, Chandigarh, India

A. Bhardwaj, B.C. Choudhary, R.B. Garg, M. Gola, S. Keshri, Ashok Kumar, S. Malhotra, M. Naimuddin, P. Priyanka, K. Ranjan, Aashaq Shah, R. Sharma

University of Delhi, Delhi, India

R. Bhardwaj [24], M. Bharti, R. Bhattacharya, S. Bhattacharya, U. Bhawandeep [24], D. Bhowmik, S. Dey, S. Dutt [24], S. Dutta, S. Ghosh, K. Mondal, S. Nandan, A. Purohit, P.K. Rout, A. Roy, S. Roy Chowdhury, S. Sarkar, M. Sharan, B. Singh, S. Thakur [24]

Saha Institute of Nuclear Physics, HBNI, Kolkata, India

P.K. Behera

Indian Institute of Technology Madras, Madras, India

R. Chudasama, D. Dutta, V. Jha, V. Kumar, P.K. Netrakanti, L.M. Pant, P. Shukla

Bhabha Atomic Research Centre, Mumbai, India

T. Aziz, M.A. Bhat, S. Dugad, G.B. Mohanty, N. Sur, B. Sutar, R.K. Verma

Tata Institute of Fundamental Research-A, Mumbai, India

S. Banerjee, S. Bhattacharya, S. Chatterjee, P. Das, M. Guchait, Sa. Jain, S. Karmakar, S. Kumar, M. Maity [25], G. Majumder, K. Mazumdar, N. Sahoo, T. Sarkar [25]

Tata Institute of Fundamental Research-B, Mumbai, India

S. Chauhan, S. Dube, V. Hegde, A. Kapoor, K. Kothekar, S. Pandey, A. Rane, S. Sharma

Indian Institute of Science Education and Research (IISER), Pune, India

S. Chenarani [26], E. Eskandari Tadavani, S.M. Etesami [26], M. Khakzad, M. Mohammadi Najafabadi, M. Naseri, F. Rezaei Hosseinabadi, B. Safarzadeh [27], M. Zeinali

Institute for Research in Fundamental Sciences (IPM), Tehran, Iran

M. Felcini, M. Grunewald

University College Dublin, Dublin, Ireland

M. Abbrescia [a,b], C. Calabria [a,b], A. Colaleo [a], D. Creanza [a,c], L. Cristella [a,b], N. De Filippis [a,c], M. De Palma [a,b], A. Di Florio [a,b], F. Errico [a,b], L. Fiore [a], A. Gelmi [a,b], G. Iaselli [a,c], M. Ince [a,b], S. Lezki [a,b], G. Maggi [a,c], M. Maggi [a], G. Miniello [a,b], S. My [a,b], S. Nuzzo [a,b], A. Pompili [a,b], G. Pugliese [a,c], R. Radogna [a], A. Ranieri [a], G. Selvaggi [a,b], A. Sharma [a], L. Silvestris [a], R. Venditti [a], P. Verwilligen [a], G. Zito [a]

[a] *INFN Sezione di Bari, Bari, Italy*
[b] *Università di Bari, Bari, Italy*
[c] *Politecnico di Bari, Bari, Italy*

G. Abbiendi [a], C. Battilana [a,b], D. Bonacorsi [a,b], L. Borgonovi [a,b], S. Braibant-Giacomelli [a,b], R. Campanini [a,b], P. Capiluppi [a,b], A. Castro [a,b], F.R. Cavallo [a], S.S. Chhibra [a,b], C. Ciocca [a], G. Codispoti [a,b], M. Cuffiani [a,b], G.M. Dallavalle [a], F. Fabbri [a], A. Fanfani [a,b], P. Giacomelli [a], C. Grandi [a], L. Guiducci [a,b], F. Iemmi [a,b], S. Marcellini [a], G. Masetti [a], A. Montanari [a], F.L. Navarria [a,b], A. Perrotta [a], F. Primavera [a,b,15], A.M. Rossi [a,b], T. Rovelli [a,b], G.P. Siroli [a,b], N. Tosi [a]

[a] *INFN Sezione di Bologna, Bologna, Italy*
[b] *Università di Bologna, Bologna, Italy*

S. Albergo [a,b], A. Di Mattia [a], R. Potenza [a,b], A. Tricomi [a,b], C. Tuve [a,b]

[a] *INFN Sezione di Catania, Catania, Italy*
[b] *Università di Catania, Catania, Italy*

G. Barbagli [a], K. Chatterjee [a,b], V. Ciulli [a,b], C. Civinini [a], R. D'Alessandro [a,b], E. Focardi [a,b], G. Latino, P. Lenzi [a,b], M. Meschini [a], S. Paoletti [a], L. Russo [a,28], G. Sguazzoni [a], D. Strom [a], L. Viliani [a]

[a] *INFN Sezione di Firenze, Firenze, Italy*
[b] *Università di Firenze, Firenze, Italy*

L. Benussi, S. Bianco, F. Fabbri, D. Piccolo

INFN Laboratori Nazionali di Frascati, Frascati, Italy

F. Ferro [a], F. Ravera [a,b], E. Robutti [a], S. Tosi [a,b]

[a] *INFN Sezione di Genova, Genova, Italy*
[b] *Università di Genova, Genova, Italy*

A. Benaglia [a], A. Beschi [b], L. Brianza [a,b], F. Brivio [a,b], V. Ciriolo [a,b,15], S. Di Guida [a,b,15], M.E. Dinardo [a,b], S. Fiorendi [a,b], S. Gennai [a], A. Ghezzi [a,b], P. Govoni [a,b], M. Malberti [a,b], S. Malvezzi [a], A. Massironi [a,b], D. Menasce [a], L. Moroni [a], M. Paganoni [a,b], D. Pedrini [a], S. Ragazzi [a,b], T. Tabarelli de Fatis [a,b]

[a] *INFN Sezione di Milano-Bicocca, Milano, Italy*
[b] *Università di Milano-Bicocca, Milano, Italy*

S. Buontempo [a], N. Cavallo [a,c], A. Di Crescenzo [a,b], F. Fabozzi [a,c], F. Fienga [a], G. Galati [a], A.O.M. Iorio [a,b], W.A. Khan [a], L. Lista [a], S. Meola [a,d,15], P. Paolucci [a,15], C. Sciacca [a,b], E. Voevodina [a,b]

[a] *INFN Sezione di Napoli, Napoli, Italy*
[b] *Università di Napoli 'Federico II', Napoli, Italy*
[c] *Università della Basilicata, Potenza, Italy*
[d] *Università G. Marconi, Roma, Italy*

P. Azzi [a], N. Bacchetta [a], M. Bellato [a], D. Bisello [a,b], A. Boletti [a,b], A. Bragagnolo, R. Carlin [a,b], P. Checchia [a], M. Dall'Osso [a,b], P. De Castro Manzano [a], T. Dorigo [a], U. Gasparini [a,b], A. Gozzelino [a], S. Lacaprara [a], P. Lujan, M. Margoni [a,b], A.T. Meneguzzo [a,b], J. Pazzini [a,b], N. Pozzobon [a,b], P. Ronchese [a,b], R. Rossin [a,b], F. Simonetto [a,b], A. Tiko, E. Torassa [a], M. Zanetti [a,b], P. Zotto [a,b], G. Zumerle [a,b]

[a] *INFN Sezione di Padova, Padova, Italy*
[b] *Università di Padova, Padova, Italy*
[c] *Università di Trento, Trento, Italy*

A. Braghieri [a], A. Magnani [a], P. Montagna [a,b], S.P. Ratti [a,b], V. Re [a], M. Ressegotti [a,b], C. Riccardi [a,b], P. Salvini [a], I. Vai [a,b], P. Vitulo [a,b]

[a] INFN Sezione di Pavia, Pavia, Italy
[b] Università di Pavia, Pavia, Italy

L. Alunni Solestizi [a,b], M. Biasini [a,b], G.M. Bilei [a], C. Cecchi [a,b], D. Ciangottini [a,b], L. Fanò [a,b], P. Lariccia [a,b], R. Leonardi [a,b], E. Manoni [a], G. Mantovani [a,b], V. Mariani [a,b], M. Menichelli [a], A. Rossi [a,b], A. Santocchia [a,b], D. Spiga [a]

[a] INFN Sezione di Perugia, Perugia, Italy
[b] Università di Perugia, Perugia, Italy

K. Androsov [a], P. Azzurri [a], G. Bagliesi [a], L. Bianchini [a], T. Boccali [a], L. Borrello, R. Castaldi [a], M.A. Ciocci [a,b], R. Dell'Orso [a], G. Fedi [a], F. Fiori [a,c], L. Giannini [a,c], A. Giassi [a], M.T. Grippo [a], F. Ligabue [a,c], E. Manca [a,c], G. Mandorli [a,c], A. Messineo [a,b], F. Palla [a], A. Rizzi [a,b], P. Spagnolo [a], R. Tenchini [a], G. Tonelli [a,b], A. Venturi [a], P.G. Verdini [a]

[a] INFN Sezione di Pisa, Pisa, Italy
[b] Università di Pisa, Pisa, Italy
[c] Scuola Normale Superiore di Pisa, Pisa, Italy

L. Barone [a,b], F. Cavallari [a], M. Cipriani [a,b], N. Daci [a], D. Del Re [a,b], E. Di Marco [a,b], M. Diemoz [a], S. Gelli [a,b], E. Longo [a,b], B. Marzocchi [a,b], P. Meridiani [a], G. Organtini [a,b], F. Pandolfi [a], R. Paramatti [a,b], F. Preiato [a,b], S. Rahatlou [a,b], C. Rovelli [a], F. Santanastasio [a,b]

[a] INFN Sezione di Roma, Rome, Italy
[b] Sapienza Università di Roma, Rome, Italy

N. Amapane [a,b], R. Arcidiacono [a,c], S. Argiro [a,b], M. Arneodo [a,c], N. Bartosik [a], R. Bellan [a,b], C. Biino [a], N. Cartiglia [a], F. Cenna [a,b], S. Cometti, M. Costa [a,b], R. Covarelli [a,b], N. Demaria [a], B. Kiani [a,b], C. Mariotti [a], S. Maselli [a], E. Migliore [a,b], V. Monaco [a,b], E. Monteil [a,b], M. Monteno [a], M.M. Obertino [a,b], L. Pacher [a,b], N. Pastrone [a], M. Pelliccioni [a], G.L. Pinna Angioni [a,b], A. Romero [a,b], M. Ruspa [a,c], R. Sacchi [a,b], K. Shchelina [a,b], V. Sola [a], A. Solano [a,b], D. Soldi, A. Staiano [a]

[a] INFN Sezione di Torino, Torino, Italy
[b] Università di Torino, Torino, Italy
[c] Università del Piemonte Orientale, Novara, Italy

S. Belforte [a], V. Candelise [a,b], M. Casarsa [a], F. Cossutti [a], G. Della Ricca [a,b], F. Vazzoler [a,b], A. Zanetti [a]

[a] INFN Sezione di Trieste, Trieste, Italy
[b] Università di Trieste, Trieste, Italy

D.H. Kim, G.N. Kim, M.S. Kim, J. Lee, S. Lee, S.W. Lee, C.S. Moon, Y.D. Oh, S. Sekmen, D.C. Son, Y.C. Yang

Kyungpook National University, Daegu, Republic of Korea

H. Kim, D.H. Moon, G. Oh

Chonnam National University, Institute for Universe and Elementary Particles, Kwangju, Republic of Korea

J. Goh [29], T.J. Kim

Hanyang University, Seoul, Republic of Korea

S. Cho, S. Choi, Y. Go, D. Gyun, S. Ha, B. Hong, Y. Jo, K. Lee, K.S. Lee, S. Lee, J. Lim, S.K. Park, Y. Roh

Korea University, Seoul, Republic of Korea

H.S. Kim

Sejong University, Seoul, Republic of Korea

J. Almond, J. Kim, J.S. Kim, H. Lee, K. Lee, K. Nam, S.B. Oh, B.C. Radburn-Smith, S.h. Seo, U.K. Yang, H.D. Yoo, G.B. Yu

Seoul National University, Seoul, Republic of Korea

D. Jeon, H. Kim, J.H. Kim, J.S.H. Lee, I.C. Park

University of Seoul, Seoul, Republic of Korea

Y. Choi, C. Hwang, J. Lee, I. Yu

Sungkyunkwan University, Suwon, Republic of Korea

V. Dudenas, A. Juodagalvis, J. Vaitkus

Vilnius University, Vilnius, Lithuania

I. Ahmed, Z.A. Ibrahim, M.A.B. Md Ali [30], F. Mohamad Idris [31], W.A.T. Wan Abdullah, M.N. Yusli, Z. Zolkapli

National Centre for Particle Physics, Universiti Malaya, Kuala Lumpur, Malaysia

A. Castaneda Hernandez, J.A. Murillo Quijada

Universidad de Sonora (UNISON), Hermosillo, Mexico

H. Castilla-Valdez, E. De La Cruz-Burelo, M.C. Duran-Osuna, I. Heredia-De La Cruz [32], R. Lopez-Fernandez, J. Mejia Guisao, R.I. Rabadan-Trejo, M. Ramirez-Garcia, G. Ramirez-Sanchez, R. Reyes-Almanza, A. Sanchez-Hernandez

Centro de Investigacion y de Estudios Avanzados del IPN, Mexico City, Mexico

S. Carrillo Moreno, C. Oropeza Barrera, F. Vazquez Valencia

Universidad Iberoamericana, Mexico City, Mexico

J. Eysermans, I. Pedraza, H.A. Salazar Ibarguen, C. Uribe Estrada

Benemerita Universidad Autonoma de Puebla, Puebla, Mexico

A. Morelos Pineda

Universidad Autónoma de San Luis Potosí, San Luis Potosí, Mexico

D. Krofcheck

University of Auckland, Auckland, New Zealand

S. Bheesette, P.H. Butler

University of Canterbury, Christchurch, New Zealand

A. Ahmad, M. Ahmad, M.I. Asghar, Q. Hassan, H.R. Hoorani, A. Saddique, M.A. Shah, M. Shoaib, M. Waqas

National Centre for Physics, Quaid-I-Azam University, Islamabad, Pakistan

H. Bialkowska, M. Bluj, B. Boimska, T. Frueboes, M. Górski, M. Kazana, K. Nawrocki, M. Szleper, P. Traczyk, P. Zalewski

National Centre for Nuclear Research, Swierk, Poland

K. Bunkowski, A. Byszuk [33], K. Doroba, A. Kalinowski, M. Konecki, J. Krolikowski, M. Misiura, M. Olszewski, A. Pyskir, M. Walczak

Institute of Experimental Physics, Faculty of Physics, University of Warsaw, Warsaw, Poland

P. Bargassa, C. Beirão Da Cruz E Silva, A. Di Francesco, P. Faccioli, B. Galinhas, M. Gallinaro, J. Hollar, N. Leonardo, L. Lloret Iglesias, M.V. Nemallapudi, J. Seixas, G. Strong, O. Toldaiev, D. Vadruccio, J. Varela

Laboratório de Instrumentação e Física Experimental de Partículas, Lisboa, Portugal

S. Afanasiev, V. Alexakhin, P. Bunin, M. Gavrilenko, A. Golunov, I. Golutvin, N. Gorbounov, V. Karjavin, A. Lanev, A. Malakhov, V. Matveev [34,35], P. Moisenz, V. Palichik, V. Perelygin, M. Savina, S. Shmatov, V. Smirnov, N. Voytishin, A. Zarubin

Joint Institute for Nuclear Research, Dubna, Russia

V. Golovtsov, Y. Ivanov, V. Kim [36], E. Kuznetsova [37], P. Levchenko, V. Murzin, V. Oreshkin, I. Smirnov, D. Sosnov, V. Sulimov, L. Uvarov, S. Vavilov, A. Vorobyev

Petersburg Nuclear Physics Institute, Gatchina (St. Petersburg), Russia

Yu. Andreev, A. Dermenev, S. Gninenko, N. Golubev, A. Karneyeu, M. Kirsanov, N. Krasnikov, A. Pashenkov, D. Tlisov, A. Toropin

Institute for Nuclear Research, Moscow, Russia

V. Epshteyn, V. Gavrilov, N. Lychkovskaya, V. Popov, I. Pozdnyakov, G. Safronov, A. Spiridonov, A. Stepennov, V. Stolin, M. Toms, E. Vlasov, A. Zhokin

Institute for Theoretical and Experimental Physics, Moscow, Russia

T. Aushev

Moscow Institute of Physics and Technology, Moscow, Russia

M. Chadeeva [38], P. Parygin, D. Philippov, S. Polikarpov [38], E. Popova, V. Rusinov

National Research Nuclear University 'Moscow Engineering Physics Institute' (MEPhI), Moscow, Russia

V. Andreev, M. Azarkin [35], I. Dremin [35], M. Kirakosyan [35], S.V. Rusakov, A. Terkulov

P.N. Lebedev Physical Institute, Moscow, Russia

A. Baskakov, A. Belyaev, E. Boos, M. Dubinin [39], L. Dudko, A. Ershov, A. Gribushin, V. Klyukhin, O. Kodolova, I. Lokhtin, I. Miagkov, S. Obraztsov, S. Petrushanko, V. Savrin, A. Snigirev

Skobeltsyn Institute of Nuclear Physics, Lomonosov Moscow State University, Moscow, Russia

V. Blinov [40], T. Dimova [40], L. Kardapoltsev [40], D. Shtol [40], Y. Skovpen [40]

Novosibirsk State University (NSU), Novosibirsk, Russia

I. Azhgirey, I. Bayshev, S. Bitioukov, D. Elumakhov, A. Godizov, V. Kachanov, A. Kalinin, D. Konstantinov, P. Mandrik, V. Petrov, R. Ryutin, S. Slabospitskii, A. Sobol, S. Troshin, N. Tyurin, A. Uzunian, A. Volkov

Institute for High Energy Physics of National Research Centre 'Kurchatov Institute', Protvino, Russia

A. Babaev, S. Baidali, V. Okhotnikov

National Research Tomsk Polytechnic University, Tomsk, Russia

P. Adzic [41], P. Cirkovic, D. Devetak, M. Dordevic, J. Milosevic

University of Belgrade, Faculty of Physics and Vinca Institute of Nuclear Sciences, Belgrade, Serbia

J. Alcaraz Maestre, A. Álvarez Fernández, I. Bachiller, M. Barrio Luna, J.A. Brochero Cifuentes, M. Cerrada, N. Colino, B. De La Cruz, A. Delgado Peris, C. Fernandez Bedoya, J.P. Fernández Ramos, J. Flix, M.C. Fouz, O. Gonzalez Lopez, S. Goy Lopez, J.M. Hernandez, M.I. Josa, D. Moran, A. Pérez-Calero Yzquierdo, J. Puerta Pelayo, I. Redondo, L. Romero, M.S. Soares, A. Triossi

Centro de Investigaciones Energéticas Medioambientales y Tecnológicas (CIEMAT), Madrid, Spain

C. Albajar, J.F. de Trocóniz

Universidad Autónoma de Madrid, Madrid, Spain

J. Cuevas, C. Erice, J. Fernandez Menendez, S. Folgueras, I. Gonzalez Caballero, J.R. González Fernández, E. Palencia Cortezon, V. Rodríguez Bouza, S. Sanchez Cruz, P. Vischia, J.M. Vizan Garcia

Universidad de Oviedo, Oviedo, Spain

I.J. Cabrillo, A. Calderon, B. Chazin Quero, J. Duarte Campderros, M. Fernandez, P.J. Fernández Manteca, A. García Alonso, J. Garcia-Ferrero, G. Gomez, A. Lopez Virto, J. Marco, C. Martinez Rivero, P. Martinez Ruiz del Arbol, F. Matorras, J. Piedra Gomez, C. Prieels, T. Rodrigo, A. Ruiz-Jimeno, L. Scodellaro, N. Trevisani, I. Vila, R. Vilar Cortabitarte

Instituto de Física de Cantabria (IFCA), CSIC-Universidad de Cantabria, Santander, Spain

D. Abbaneo, B. Akgun, E. Auffray, P. Baillon, A.H. Ball, D. Barney, J. Bendavid, M. Bianco, A. Bocci, C. Botta, E. Brondolin, T. Camporesi, M. Cepeda, G. Cerminara, E. Chapon, Y. Chen, G. Cucciati, D. d'Enterria, A. Dabrowski, V. Daponte, A. David, A. De Roeck, N. Deelen, M. Dobson, M. Dünser, N. Dupont, A. Elliott-Peisert, P. Everaerts, F. Fallavollita [42], D. Fasanella, G. Franzoni, J. Fulcher, W. Funk, D. Gigi, A. Gilbert, K. Gill, F. Glege, M. Guilbaud, D. Gulhan, J. Hegeman, V. Innocente, A. Jafari, P. Janot, O. Karacheban [18], J. Kieseler, A. Kornmayer, M. Krammer [1], C. Lange, P. Lecoq, C. Lourenço, L. Malgeri, M. Mannelli, F. Meijers, J.A. Merlin, S. Mersi, E. Meschi, P. Milenovic [43], F. Moortgat, M. Mulders, J. Ngadiuba, S. Orfanelli, L. Orsini, F. Pantaleo [15], L. Pape, E. Perez, M. Peruzzi, A. Petrilli, G. Petrucciani, A. Pfeiffer, M. Pierini, F.M. Pitters, D. Rabady, A. Racz, T. Reis, G. Rolandi [44], M. Rovere, H. Sakulin, C. Schäfer, C. Schwick, M. Seidel, M. Selvaggi, A. Sharma, P. Silva, P. Sphicas [45], A. Stakia, J. Steggemann, M. Tosi, D. Treille, A. Tsirou, V. Veckalns [46], W.D. Zeuner

CERN, European Organization for Nuclear Research, Geneva, Switzerland

L. Caminada [47], K. Deiters, W. Erdmann, R. Horisberger, Q. Ingram, H.C. Kaestli, D. Kotlinski, U. Langenegger, T. Rohe, S.A. Wiederkehr

Paul Scherrer Institut, Villigen, Switzerland

M. Backhaus, L. Bäni, P. Berger, N. Chernyavskaya, G. Dissertori, M. Dittmar, M. Donegà, C. Dorfer, C. Grab, C. Heidegger, D. Hits, J. Hoss, T. Klijnsma, W. Lustermann, R.A. Manzoni, M. Marionneau, M.T. Meinhard, F. Micheli, P. Musella, F. Nessi-Tedaldi, J. Pata, F. Pauss, G. Perrin, L. Perrozzi, S. Pigazzini, M. Quittnat, D. Ruini, D.A. Sanz Becerra, M. Schönenberger, L. Shchutska, V.R. Tavolaro, K. Theofilatos, M.L. Vesterbacka Olsson, R. Wallny, D.H. Zhu

ETH Zurich – Institute for Particle Physics and Astrophysics (IPA), Zurich, Switzerland

T.K. Aarrestad, C. Amsler [48], D. Brzhechko, M.F. Canelli, A. De Cosa, R. Del Burgo, S. Donato, C. Galloni, T. Hreus, B. Kilminster, I. Neutelings, D. Pinna, G. Rauco, P. Robmann, D. Salerno, K. Schweiger, C. Seitz, Y. Takahashi, A. Zucchetta

Universität Zürich, Zurich, Switzerland

Y.H. Chang, K.y. Cheng, T.H. Doan, Sh. Jain, R. Khurana, C.M. Kuo, W. Lin, A. Pozdnyakov, S.S. Yu

National Central University, Chung-Li, Taiwan

P. Chang, Y. Chao, K.F. Chen, P.H. Chen, W.-S. Hou, Arun Kumar, Y.y. Li, Y.F. Liu, R.-S. Lu, E. Paganis, A. Psallidas, A. Steen, J.f. Tsai

National Taiwan University (NTU), Taipei, Taiwan

B. Asavapibhop, N. Srimanobhas, N. Suwonjandee

Chulalongkorn University, Faculty of Science, Department of Physics, Bangkok, Thailand

A. Bat, F. Boran, S. Cerci [49], S. Damarseckin, Z.S. Demiroglu, F. Dolek, C. Dozen, I. Dumanoglu, S. Girgis, G. Gokbulut, Y. Guler, E. Gurpinar, I. Hos [50], C. Isik, E.E. Kangal [51], O. Kara, A. Kayis Topaksu, U. Kiminsu, M. Oglakci, G. Onengut, K. Ozdemir [52], S. Ozturk [53], A. Polatoz, B. Tali [49], U.G. Tok, S. Turkcapar, I.S. Zorbakir, C. Zorbilmez

Çukurova University, Physics Department, Science and Art Faculty, Adana, Turkey

B. Isildak [54], G. Karapinar [55], M. Yalvac, M. Zeyrek

Middle East Technical University, Physics Department, Ankara, Turkey

I.O. Atakisi, E. Gülmez, M. Kaya [56], O. Kaya [57], S. Ozkorucuklu [58], S. Tekten, E.A. Yetkin [59]

Bogazici University, Istanbul, Turkey

M.N. Agaras, S. Atay, A. Cakir, K. Cankocak, Y. Komurcu, S. Sen [60]

Istanbul Technical University, Istanbul, Turkey

B. Grynyov

Institute for Scintillation Materials of National Academy of Science of Ukraine, Kharkov, Ukraine

L. Levchuk

National Scientific Center, Kharkov Institute of Physics and Technology, Kharkov, Ukraine

F. Ball, L. Beck, J.J. Brooke, D. Burns, E. Clement, D. Cussans, O. Davignon, H. Flacher, J. Goldstein, G.P. Heath, H.F. Heath, L. Kreczko, D.M. Newbold [61], S. Paramesvaran, B. Penning, T. Sakuma, D. Smith, V.J. Smith, J. Taylor, A. Titterton

University of Bristol, Bristol, United Kingdom

K.W. Bell, A. Belyaev [62], C. Brew, R.M. Brown, D. Cieri, D.J.A. Cockerill, J.A. Coughlan, K. Harder, S. Harper, J. Linacre, E. Olaiya, D. Petyt, C.H. Shepherd-Themistocleous, A. Thea, I.R. Tomalin, T. Williams, W.J. Womersley

Rutherford Appleton Laboratory, Didcot, United Kingdom

G. Auzinger, R. Bainbridge, P. Bloch, J. Borg, S. Breeze, O. Buchmuller, A. Bundock, S. Casasso, D. Colling, L. Corpe, P. Dauncey, G. Davies, M. Della Negra, R. Di Maria, Y. Haddad, G. Hall, G. Iles, T. James, M. Komm, C. Laner, L. Lyons, A.-M. Magnan, S. Malik, A. Martelli, J. Nash [63], A. Nikitenko [7], V. Palladino, M. Pesaresi, A. Richards, A. Rose, E. Scott, C. Seez, A. Shtipliyski, G. Singh, M. Stoye, T. Strebler, S. Summers, A. Tapper, K. Uchida, T. Virdee [15], N. Wardle, D. Winterbottom, J. Wright, S.C. Zenz

Imperial College, London, United Kingdom

J.E. Cole, P.R. Hobson, A. Khan, P. Kyberd, C.K. Mackay, A. Morton, I.D. Reid, L. Teodorescu, S. Zahid

Brunel University, Uxbridge, United Kingdom

K. Call, J. Dittmann, K. Hatakeyama, H. Liu, C. Madrid, B. Mcmaster, N. Pastika, C. Smith

Baylor University, Waco, USA

R. Bartek, A. Dominguez

Catholic University of America, Washington DC, USA

A. Buccilli, S.I. Cooper, C. Henderson, P. Rumerio, C. West

The University of Alabama, Tuscaloosa, USA

D. Arcaro, T. Bose, D. Gastler, D. Rankin, C. Richardson, J. Rohlf, L. Sulak, D. Zou

Boston University, Boston, USA

G. Benelli, X. Coubez, D. Cutts, M. Hadley, J. Hakala, U. Heintz, J.M. Hogan [64], K.H.M. Kwok, E. Laird, G. Landsberg, J. Lee, Z. Mao, M. Narain, S. Piperov, S. Sagir [65], R. Syarif, E. Usai, D. Yu

Brown University, Providence, USA

R. Band, C. Brainerd, R. Breedon, D. Burns, M. Calderon De La Barca Sanchez, M. Chertok, J. Conway, R. Conway, P.T. Cox, R. Erbacher, C. Flores, G. Funk, W. Ko, O. Kukral, R. Lander, C. Mclean, M. Mulhearn, D. Pellett, J. Pilot, S. Shalhout, M. Shi, D. Stolp, D. Taylor, K. Tos, M. Tripathi, Z. Wang, F. Zhang

University of California, Davis, Davis, USA

M. Bachtis, C. Bravo, R. Cousins, A. Dasgupta, A. Florent, J. Hauser, M. Ignatenko, N. Mccoll, S. Regnard, D. Saltzberg, C. Schnaible, V. Valuev

University of California, Los Angeles, USA

E. Bouvier, K. Burt, R. Clare, J.W. Gary, S.M.A. Ghiasi Shirazi, G. Hanson, G. Karapostoli, E. Kennedy, F. Lacroix, O.R. Long, M. Olmedo Negrete, M.I. Paneva, W. Si, L. Wang, H. Wei, S. Wimpenny, B.R. Yates

University of California, Riverside, Riverside, USA

J.G. Branson, S. Cittolin, M. Derdzinski, R. Gerosa, D. Gilbert, B. Hashemi, A. Holzner, D. Klein, G. Kole, V. Krutelyov, J. Letts, M. Masciovecchio, D. Olivito, S. Padhi, M. Pieri, M. Sani, V. Sharma, S. Simon, M. Tadel, A. Vartak, S. Wasserbaech [66], J. Wood, F. Würthwein, A. Yagil, G. Zevi Della Porta

University of California, San Diego, La Jolla, USA

N. Amin, R. Bhandari, J. Bradmiller-Feld, C. Campagnari, M. Citron, A. Dishaw, V. Dutta, M. Franco Sevilla, L. Gouskos, R. Heller, J. Incandela, A. Ovcharova, H. Qu, J. Richman, D. Stuart, I. Suarez, S. Wang, J. Yoo

University of California, Santa Barbara – Department of Physics, Santa Barbara, USA

D. Anderson, A. Bornheim, J.M. Lawhorn, H.B. Newman, T.Q. Nguyen, M. Spiropulu, J.R. Vlimant, R. Wilkinson, S. Xie, Z. Zhang, R.Y. Zhu

California Institute of Technology, Pasadena, USA

M.B. Andrews, T. Ferguson, T. Mudholkar, M. Paulini, M. Sun, I. Vorobiev, M. Weinberg

Carnegie Mellon University, Pittsburgh, USA

J.P. Cumalat, W.T. Ford, F. Jensen, A. Johnson, M. Krohn, S. Leontsinis, E. MacDonald, T. Mulholland, K. Stenson, K.A. Ulmer, S.R. Wagner

University of Colorado Boulder, Boulder, USA

J. Alexander, J. Chaves, Y. Cheng, J. Chu, A. Datta, K. Mcdermott, N. Mirman, J.R. Patterson, D. Quach, A. Rinkevicius, A. Ryd, L. Skinnari, L. Soffi, S.M. Tan, Z. Tao, J. Thom, J. Tucker, P. Wittich, M. Zientek

Cornell University, Ithaca, USA

S. Abdullin, M. Albrow, M. Alyari, G. Apollinari, A. Apresyan, A. Apyan, S. Banerjee, L.A.T. Bauerdick, A. Beretvas, J. Berryhill, P.C. Bhat, G. Bolla [†], K. Burkett, J.N. Butler, A. Canepa, G.B. Cerati, H.W.K. Cheung, F. Chlebana, M. Cremonesi, J. Duarte, V.D. Elvira, J. Freeman, Z. Gecse, E. Gottschalk, L. Gray, D. Green, S. Grünendahl, O. Gutsche, J. Hanlon, R.M. Harris, S. Hasegawa, J. Hirschauer, Z. Hu, B. Jayatilaka, S. Jindariani, M. Johnson, U. Joshi, B. Klima, M.J. Kortelainen, B. Kreis, S. Lammel, D. Lincoln, R. Lipton, M. Liu, T. Liu, J. Lykken, K. Maeshima, J.M. Marraffino, D. Mason, P. McBride, P. Merkel, S. Mrenna, S. Nahn, V. O'Dell, K. Pedro, C. Pena, O. Prokofyev, G. Rakness, L. Ristori, A. Savoy-Navarro [67],

B. Schneider, E. Sexton-Kennedy, A. Soha, W.J. Spalding, L. Spiegel, S. Stoynev, J. Strait, N. Strobbe, L. Taylor, S. Tkaczyk, N.V. Tran, L. Uplegger, E.W. Vaandering, C. Vernieri, M. Verzocchi, R. Vidal, M. Wang, H.A. Weber, A. Whitbeck

Fermi National Accelerator Laboratory, Batavia, USA

D. Acosta, P. Avery, P. Bortignon, D. Bourilkov, A. Brinkerhoff, L. Cadamuro, A. Carnes, M. Carver, D. Curry, R.D. Field, S.V. Gleyzer, B.M. Joshi, J. Konigsberg, A. Korytov, P. Ma, K. Matchev, H. Mei, G. Mitselmakher, K. Shi, D. Sperka, J. Wang, S. Wang

University of Florida, Gainesville, USA

Y.R. Joshi, S. Linn

Florida International University, Miami, USA

A. Ackert, T. Adams, A. Askew, S. Hagopian, V. Hagopian, K.F. Johnson, T. Kolberg, G. Martinez, T. Perry, H. Prosper, A. Saha, V. Sharma, R. Yohay

Florida State University, Tallahassee, USA

M.M. Baarmand, V. Bhopatkar, S. Colafranceschi, M. Hohlmann, D. Noonan, M. Rahmani, T. Roy, F. Yumiceva

Florida Institute of Technology, Melbourne, USA

M.R. Adams, L. Apanasevich, D. Berry, R.R. Betts, R. Cavanaugh, X. Chen, S. Dittmer, O. Evdokimov, C.E. Gerber, D.A. Hangal, D.J. Hofman, K. Jung, J. Kamin, C. Mills, I.D. Sandoval Gonzalez, M.B. Tonjes, N. Varelas, H. Wang, X. Wang, Z. Wu, J. Zhang

University of Illinois at Chicago (UIC), Chicago, USA

M. Alhusseini, B. Bilki [68], W. Clarida, K. Dilsiz [69], S. Durgut, R.P. Gandrajula, M. Haytmyradov, V. Khristenko, J.-P. Merlo, A. Mestvirishvili, A. Moeller, J. Nachtman, H. Ogul [70], Y. Onel, F. Ozok [71], A. Penzo, C. Snyder, E. Tiras, J. Wetzel

The University of Iowa, Iowa City, USA

B. Blumenfeld, A. Cocoros, N. Eminizer, D. Fehling, L. Feng, A.V. Gritsan, W.T. Hung, P. Maksimovic, J. Roskes, U. Sarica, M. Swartz, M. Xiao, C. You

Johns Hopkins University, Baltimore, USA

A. Al-bataineh, P. Baringer, A. Bean, S. Boren, J. Bowen, A. Bylinkin, J. Castle, S. Khalil, A. Kropivnitskaya, D. Majumder, W. Mcbrayer, M. Murray, C. Rogan, S. Sanders, E. Schmitz, J.D. Tapia Takaki, Q. Wang

The University of Kansas, Lawrence, USA

S. Duric, A. Ivanov, K. Kaadze, D. Kim, Y. Maravin, D.R. Mendis, T. Mitchell, A. Modak, A. Mohammadi, L.K. Saini, N. Skhirtladze

Kansas State University, Manhattan, USA

F. Rebassoo, D. Wright

Lawrence Livermore National Laboratory, Livermore, USA

A. Baden, O. Baron, A. Belloni, S.C. Eno, Y. Feng, C. Ferraioli, N.J. Hadley, S. Jabeen, G.Y. Jeng, R.G. Kellogg, J. Kunkle, A.C. Mignerey, F. Ricci-Tam, Y.H. Shin, A. Skuja, S.C. Tonwar, K. Wong

University of Maryland, College Park, USA

D. Abercrombie, B. Allen, V. Azzolini, A. Baty, G. Bauer, R. Bi, S. Brandt, W. Busza, I.A. Cali, M. D'Alfonso, Z. Demiragli, G. Gomez Ceballos, M. Goncharov, P. Harris, D. Hsu, M. Hu, Y. Iiyama, G.M. Innocenti, M. Klute, D. Kovalskyi, Y.-J. Lee, P.D. Luckey, B. Maier, A.C. Marini, C. Mcginn, C. Mironov, S. Narayanan, X. Niu, C. Paus, C. Roland, G. Roland, G.S.F. Stephans, K. Sumorok, K. Tatar, D. Velicanu, J. Wang, T.W. Wang, B. Wyslouch, S. Zhaozhong

Massachusetts Institute of Technology, Cambridge, USA

A.C. Benvenuti, R.M. Chatterjee, A. Evans, P. Hansen, S. Kalafut, Y. Kubota, Z. Lesko, J. Mans, S. Nourbakhsh, N. Ruckstuhl, R. Rusack, J. Turkewitz, M.A. Wadud

University of Minnesota, Minneapolis, USA

J.G. Acosta, S. Oliveros

University of Mississippi, Oxford, USA

E. Avdeeva, K. Bloom, D.R. Claes, C. Fangmeier, F. Golf, R. Gonzalez Suarez, R. Kamalieddin, I. Kravchenko, J. Monroy, J.E. Siado, G.R. Snow, B. Stieger

University of Nebraska-Lincoln, Lincoln, USA

A. Godshalk, C. Harrington, I. Iashvili, A. Kharchilava, D. Nguyen, A. Parker, S. Rappoccio, B. Roozbahani

State University of New York at Buffalo, Buffalo, USA

G. Alverson, E. Barberis, C. Freer, A. Hortiangtham, D.M. Morse, T. Orimoto, R. Teixeira De Lima, T. Wamorkar, B. Wang, A. Wisecarver, D. Wood

Northeastern University, Boston, USA

S. Bhattacharya, O. Charaf, K.A. Hahn, N. Mucia, N. Odell, M.H. Schmitt, K. Sung, M. Trovato, M. Velasco

Northwestern University, Evanston, USA

R. Bucci, N. Dev, M. Hildreth, K. Hurtado Anampa, C. Jessop, D.J. Karmgard, N. Kellams, K. Lannon, W. Li, N. Loukas, N. Marinelli, F. Meng, C. Mueller, Y. Musienko [34], M. Planer, A. Reinsvold, R. Ruchti, P. Siddireddy, G. Smith, S. Taroni, M. Wayne, A. Wightman, M. Wolf, A. Woodard

University of Notre Dame, Notre Dame, USA

J. Alimena, L. Antonelli, B. Bylsma, L.S. Durkin, S. Flowers, B. Francis, A. Hart, C. Hill, W. Ji, T.Y. Ling, W. Luo, B.L. Winer, H.W. Wulsin

The Ohio State University, Columbus, USA

S. Cooperstein, P. Elmer, J. Hardenbrook, P. Hebda, S. Higginbotham, A. Kalogeropoulos, D. Lange, M.T. Lucchini, J. Luo, D. Marlow, K. Mei, I. Ojalvo, J. Olsen, C. Palmer, P. Piroué, J. Salfeld-Nebgen, D. Stickland, C. Tully

Princeton University, Princeton, USA

S. Malik, S. Norberg

University of Puerto Rico, Mayaguez, USA

A. Barker, V.E. Barnes, S. Das, L. Gutay, M. Jones, A.W. Jung, A. Khatiwada, B. Mahakud, D.H. Miller, N. Neumeister, C.C. Peng, H. Qiu, J.F. Schulte, J. Sun, F. Wang, R. Xiao, W. Xie

Purdue University, West Lafayette, USA

T. Cheng, J. Dolen, N. Parashar

Purdue University Northwest, Hammond, USA

Z. Chen, K.M. Ecklund, S. Freed, F.J.M. Geurts, M. Kilpatrick, W. Li, B. Michlin, B.P. Padley, J. Roberts, J. Rorie, W. Shi, Z. Tu, J. Zabel, A. Zhang

Rice University, Houston, USA

A. Bodek, P. de Barbaro, R. Demina, Y.t. Duh, J.L. Dulemba, C. Fallon, T. Ferbel, M. Galanti, A. Garcia-Bellido, J. Han, O. Hindrichs, A. Khukhunaishvili, K.H. Lo, P. Tan, R. Taus, M. Verzetti

University of Rochester, Rochester, USA

A. Agapitos, J.P. Chou, Y. Gershtein, T.A. Gómez Espinosa, E. Halkiadakis, M. Heindl, E. Hughes, S. Kaplan, R. Kunnawalkam Elayavalli, S. Kyriacou, A. Lath, R. Montalvo, K. Nash, M. Osherson, H. Saka, S. Salur, S. Schnetzer, D. Sheffield, S. Somalwar, R. Stone, S. Thomas, P. Thomassen, M. Walker

Rutgers, The State University of New Jersey, Piscataway, USA

A.G. Delannoy, J. Heideman, G. Riley, S. Spanier, K. Thapa

University of Tennessee, Knoxville, USA

O. Bouhali [72], A. Celik, M. Dalchenko, M. De Mattia, A. Delgado, S. Dildick, R. Eusebi, J. Gilmore, T. Huang, T. Kamon [73], S. Luo, R. Mueller, R. Patel, A. Perloff, L. Perniè, D. Rathjens, A. Safonov

Texas A&M University, College Station, USA

N. Akchurin, J. Damgov, F. De Guio, P.R. Dudero, S. Kunori, K. Lamichhane, S.W. Lee, T. Mengke, S. Muthumuni, T. Peltola, S. Undleeb, I. Volobouev, Z. Wang

Texas Tech University, Lubbock, USA

S. Greene, A. Gurrola, R. Janjam, W. Johns, C. Maguire, A. Melo, H. Ni, K. Padeken, J.D. Ruiz Alvarez, P. Sheldon, S. Tuo, J. Velkovska, M. Verweij, Q. Xu

Vanderbilt University, Nashville, USA

M.W. Arenton, P. Barria, B. Cox, R. Hirosky, M. Joyce, A. Ledovskoy, H. Li, C. Neu, T. Sinthuprasith, Y. Wang, E. Wolfe, F. Xia

University of Virginia, Charlottesville, USA

R. Harr, P.E. Karchin, N. Poudyal, J. Sturdy, P. Thapa, S. Zaleski

Wayne State University, Detroit, USA

M. Brodski, J. Buchanan, C. Caillol, D. Carlsmith, S. Dasu, L. Dodd, B. Gomber, M. Grothe, M. Herndon, A. Hervé, U. Hussain, P. Klabbers, A. Lanaro, A. Levine, K. Long, R. Loveless, T. Ruggles, A. Savin, N. Smith, W.H. Smith, N. Woods

University of Wisconsin – Madison, Madison, WI, USA

† Deceased.
[1] Also at Vienna University of Technology, Vienna, Austria.
[2] Also at IRFU, CEA, Université Paris-Saclay, Gif-sur-Yvette, France.
[3] Also at Universidade Estadual de Campinas, Campinas, Brazil.
[4] Also at Federal University of Rio Grande do Sul, Porto Alegre, Brazil.
[5] Also at Université Libre de Bruxelles, Bruxelles, Belgium.
[6] Also at University of Chinese Academy of Sciences, Beijing, China.
[7] Also at Institute for Theoretical and Experimental Physics, Moscow, Russia.
[8] Also at Joint Institute for Nuclear Research, Dubna, Russia.
[9] Also at Cairo University, Cairo, Egypt.
[10] Also at Helwan University, Cairo, Egypt.
[11] Now at Zewail City of Science and Technology, Zewail, Egypt.
[12] Also at Department of Physics, King Abdulaziz University, Jeddah, Saudi Arabia.
[13] Also at Université de Haute Alsace, Mulhouse, France.
[14] Also at Skobeltsyn Institute of Nuclear Physics, Lomonosov Moscow State University, Moscow, Russia.

[15] Also at CERN, European Organization for Nuclear Research, Geneva, Switzerland.
[16] Also at RWTH Aachen University, III. Physikalisches Institut A, Aachen, Germany.
[17] Also at University of Hamburg, Hamburg, Germany.
[18] Also at Brandenburg University of Technology, Cottbus, Germany.
[19] Also at MTA-ELTE Lendület CMS Particle and Nuclear Physics Group, Eötvös Loránd University, Budapest, Hungary.
[20] Also at Institute of Nuclear Research ATOMKI, Debrecen, Hungary.
[21] Also at Institute of Physics, University of Debrecen, Debrecen, Hungary.
[22] Also at Indian Institute of Technology Bhubaneswar, Bhubaneswar, India.
[23] Also at Institute of Physics, Bhubaneswar, India.
[24] Also at Shoolini University, Solan, India.
[25] Also at University of Visva-Bharati, Santiniketan, India.
[26] Also at Isfahan University of Technology, Isfahan, Iran.
[27] Also at Plasma Physics Research Center, Science and Research Branch, Islamic Azad University, Tehran, Iran.
[28] Also at Università degli Studi di Siena, Siena, Italy.
[29] Also at Kyunghee University, Seoul, Republic of Korea.
[30] Also at International Islamic University of Malaysia, Kuala Lumpur, Malaysia.
[31] Also at Malaysian Nuclear Agency, MOSTI, Kajang, Malaysia.
[32] Also at Consejo Nacional de Ciencia y Tecnología, Mexico city, Mexico.
[33] Also at Warsaw University of Technology, Institute of Electronic Systems, Warsaw, Poland.
[34] Also at Institute for Nuclear Research, Moscow, Russia.
[35] Now at National Research Nuclear University 'Moscow Engineering Physics Institute' (MEPhI), Moscow, Russia.
[36] Also at St. Petersburg State Polytechnical University, St. Petersburg, Russia.
[37] Also at University of Florida, Gainesville, USA.
[38] Also at P.N. Lebedev Physical Institute, Moscow, Russia.
[39] Also at California Institute of Technology, Pasadena, USA.
[40] Also at Budker Institute of Nuclear Physics, Novosibirsk, Russia.
[41] Also at Faculty of Physics, University of Belgrade, Belgrade, Serbia.
[42] Also at INFN Sezione di Pavia [a], Università di Pavia [b], Pavia, Italy.
[43] Also at University of Belgrade, Faculty of Physics and Vinca Institute of Nuclear Sciences, Belgrade, Serbia.
[44] Also at Scuola Normale e Sezione dell'INFN, Pisa, Italy.
[45] Also at National and Kapodistrian University of Athens, Athens, Greece.
[46] Also at Riga Technical University, Riga, Latvia.
[47] Also at Universität Zürich, Zurich, Switzerland.
[48] Also at Stefan Meyer Institute for Subatomic Physics (SMI), Vienna, Austria.
[49] Also at Adiyaman University, Adiyaman, Turkey.
[50] Also at Istanbul Aydin University, Istanbul, Turkey.
[51] Also at Mersin University, Mersin, Turkey.
[52] Also at Piri Reis University, Istanbul, Turkey.
[53] Also at Gaziosmanpasa University, Tokat, Turkey.
[54] Also at Ozyegin University, Istanbul, Turkey.
[55] Also at Izmir Institute of Technology, Izmir, Turkey.
[56] Also at Marmara University, Istanbul, Turkey.
[57] Also at Kafkas University, Kars, Turkey.
[58] Also at Istanbul University, Faculty of Science, Istanbul, Turkey.
[59] Also at Istanbul Bilgi University, Istanbul, Turkey.
[60] Also at Hacettepe University, Ankara, Turkey.
[61] Also at Rutherford Appleton Laboratory, Didcot, United Kingdom.
[62] Also at School of Physics and Astronomy, University of Southampton, Southampton, United Kingdom.
[63] Also at Monash University, Faculty of Science, Clayton, Australia.
[64] Also at Bethel University, St. Paul, USA.
[65] Also at Karamanoğlu Mehmetbey University, Karaman, Turkey.
[66] Also at Utah Valley University, Orem, USA.
[67] Also at Purdue University, West Lafayette, USA.
[68] Also at Beykent University, Istanbul, Turkey.
[69] Also at Bingol University, Bingol, Turkey.
[70] Also at Sinop University, Sinop, Turkey.
[71] Also at Mimar Sinan University, Istanbul, Istanbul, Turkey.
[72] Also at Texas A&M University at Qatar, Doha, Qatar.
[73] Also at Kyungpook National University, Daegu, Republic of Korea.